

Constraints on the metamorphic evolution of the eastern Himalayan syntaxis from geochronologic and petrologic studies of Namche Barwa

Amanda L. Booth^{1†}, C. Page Chamberlain¹, William S.F. Kidd², Peter K. Zeitler³

¹Water and Environmental Research Center, Institute of Northern Engineering, University of Alaska Fairbanks, P.O. Box 755860, Fairbanks, Alaska 99775, USA

²Department of Earth and Atmospheric Sciences, University at Albany, Albany, New York 12222, USA

³Department of Earth and Environmental Sciences, Lehigh University, Bethlehem, Pennsylvania 18015, USA

ABSTRACT

The eastern Himalayan syntaxis is host to the actively deforming metamorphic massif, Namche Barwa. This massif has experienced a complex history of uplift and deformation, influenced by intense fluvial erosion associated with the Yarlung Tsangpo. Here we present new thermobarometric and geochronologic information on metamorphic rocks from the Namche Barwa–Gyala Peri region. Pressure-temperature data are combined with U-Th-Pb ages of monazite and titanite in an effort to trace the metamorphic evolution of the eastern Himalaya. Metapelitic rocks containing garnet-biotite-plagioclase assemblages yield peak metamorphic pressures and temperatures of 10–14 kbar and 700–900 °C in the structural core of the massif. There is a distinct metamorphic break across the Namula thrust, separating high-grade rocks to the north from lower grade rocks to the south. Ion microprobe monazite and titanite ages of 3–10 Ma indicate that timing of metamorphism is roughly coincident with the age of granitic melt production (<10 Ma) as well as the onset of rapid denudation. In-situ ages determined from monazites included in garnet show that they grew over a period of several million years (6.4 ± 0.3 Ma to 11.3 ± 0.2 Ma) and during a pressure decrease of ~5 kbar. These data suggest that high-grade metamorphism and anatexis is a phenomenon that has been operative at Namche Barwa since at least the mid-Miocene. Geodynamic models for the evolution of Namche Barwa must therefore account for these features. We conclude that our data most closely fit the tectonic aneurysm model, based on distinct spatial correlations between pressure-temperature (P-T) conditions, age of metamorphism, and erosion by the Tsangpo.

[†]E-mail: ffa1b@uaf.edu

INTRODUCTION

Metamorphism in the Himalayas is primarily associated with Paleocene-Eocene collision of India with Asia. As such, Himalayan metamorphic rocks are generally related to convergent processes such as thrusting, crustal thickening, and lateral expulsion of material along transform fault systems (Hodges, 2000, and references therein). Synorogenic extension is also invoked as a means for producing anatexis and granulite-facies metamorphism along the South Tibetan detachment system as well as gneiss domes in southern Tibet (Chen et al., 1990; Guillot et al., 1998; Lee et al., 2000). Geomorphic processes are less commonly attributed to influencing the production of high-grade metamorphic rocks, and are only called upon in areas of the Himalaya where major rivers crosscut the orogen (i.e., Zeitler et al., 1993; Burg et al., 1998; Zeitler et al., 2001a; Vannay et al., 2004). Based on close spatial correlations between structural deformation and erosion by the Yarlung Tsangpo, Zeitler et al. (2001a) suggested that in the eastern Himalayan syntaxis these processes are linked by positive feedbacks. However, with the exception of a few studies (Zhang et al., 1992; Zhong and Ding, 1996; Liu and Zhong, 1997; Burg et al., 1998; Ding et al., 2001; Geng et al., 2006), there are limited data regarding the metamorphic evolution of the eastern Himalayan syntaxis, information that is critical in evaluating hypotheses regarding the driving force behind metamorphism of this region.

The antiformal basement massif, Namche Barwa, is located in a remote area of the eastern Himalayan syntaxis, the tectonic and metamorphic history of which is not well understood. Numerous models exist for the development of the Himalayan syntaxes, including oroclinal bending (e.g., Ratschbacher et al., 1994), lithospheric-scale folding (e.g., Treloar et al., 1991; Burg et al., 1998; Burg and Podladchikov, 1999), and duplex thrusting (e.g., Ding et al.,

2001; Yin et al., 2006). Many of these models are consistent with structural trends observed at the syntaxes, but they do not address the temporal and spatial association between young metamorphism and fluvial erosion (e.g., Zeitler et al., 1993; Zeitler et al., 2001a). In the eastern Himalaya, the Yarlung Tsangpo crosses the orogen between the peaks Namche Barwa and Gyala Peri, exposing ~7000 m of actively deforming metamorphic rocks and very young granites (<10 Ma; Burg et al., 1998; Ding et al., 2001; Zeitler et al., 2001a; Booth et al., 2004). These young melts are distinct from those reported elsewhere in the Himalayas, and correspond to a period of rapid denudation at Namche Barwa, estimated at ~10 mm/yr over the past 3 Myr (Burg et al., 1998). The coincidence of young granites with rapid denudation has been explained by the “tectonic aneurysm” model (Zeitler et al., 2001a; Koons et al., 2002), which attributes anatexis and high-grade metamorphism to rapid exhumation by the Yarlung Tsangpo. It remains unclear, however, on what length of time scale this aneurysm operates, or indeed whether such a model is applicable to the Namche Barwa region. If the origin of Namche Barwa is credited to rapid exhumation localized by river erosion, the question remains whether it is a long-term, ongoing process or merely a transient feature in the crust. An alternative model for the coincidence of intense erosion with young melts might involve ductile extrusion in association with channel flow from beneath Tibet (i.e., Beaumont et al., 2001, 2004). Here, we place constraints on these issues of time scales and geodynamical interpretations using thermobarometry and U-Th-Pb geochronology.

BACKGROUND

Geology

The eastern syntaxis of the Himalayas is expressed as a pronounced southward bend in

the crest line and the major geological units of the dominantly E-W-trending orogen. This change coincides with the high topography of the Namche Barwa region, the exposure of granulite-grade metamorphic rocks, and a 180-degree bend in the Yarlung Tsangpo. Namche Barwa comprises the eastern termination of the Himalayan orogen, and is the region in which the transition occurs between thrust-fault-dominated tectonics in the Himalayas and the strike-slip tectonic regime of Southeast Asia.

Near the peaks Namche Barwa and Gyala Peri, both Indian and Asian continental crust is exposed, separated by a narrow and highly deformed equivalent to the Indus Tsangpo suture zone (Fig. 1). This unit has been interpreted as a continuous belt of mélangé, including sporadic ultramafic and mafic lenses from a dismembered ophiolite suite (Geng et al., 2006). The Gangdese or Transhimalayan Plutonic Belt of the southern Lhasa terrane (formerly part of the Asian plate margin) consists of Cretaceous and Paleogene calc-alkaline plutons intruded into deformed Paleozoic and Mesozoic low-grade sedimentary strata, and local higher grade gneissic rocks interpreted as their basement. These units form a frame around the antiformal Namche Barwa metamorphic massif. Surrounding much of the

syntaxis, a mylonitic zone separates the Lhasa terrane rocks from the Namche Barwa core of Indian basement gneisses. Abundant amphibolites and uncommon serpentine lenses on the outer edge of this zone suggest that it marks the eastern continuation of the Indus Tsangpo suture zone, with remnants of metaophiolites separating Asian from Indian plate rocks. A distinctive belt of metasedimentary rocks (dominantly quartzites and pelites, with some calc-silicates), thought to be a more deformed and metamorphosed equivalent of the Tethyan Himalaya Paleozoic and Mesozoic sedimentary section, adjoins and also forms part of this zone of highly strained rocks. Medium- to high-grade metamorphic rocks (presumably derived from Indian basement rocks) make up the core of the Namche Barwa massif, and were once structurally below the Lhasa terrane and the other units described above. They are dominantly migmatitic gneisses of Proterozoic age (Zhang et al., 1992; Burg et al., 1998). The gneisses are divided by Geng et al. (2006) into three components: (1) layered marble and diopside-bearing calc-silicate rocks within felsic gneiss, forming the upper part of the exposed Indian plate, (2) aluminous felsic gneiss containing boudins of high-pressure granulite, forming the lower part of the Indian

plate, and (3) migmatite comprising the central part of the Namche Barwa massif.

Structure

The eastern Himalayan syntaxis represents a broad region over which structural trends in southeastern Tibet and the Himalayan orogen change in strike from E-W to N-S. This change is also evident in the trends of surface features such as major river valleys located along strike-slip faults (Hallet and Molnar, 2001), and overall the syntaxis likely reflects several generations of structural events along the eastern edge of the Indian plate, including Miocene extrusion tectonics (Wang and Burchfiel, 1997), and ongoing clockwise rotations (Burchfiel et al., 1998; Shen et al., 2001).

Namche Barwa is part of a large-scale, north-plunging antiformal structure, the hinge of which follows the present topographic crest, e.g., near Doxicong–La Pass (Fig. 2; see also Burg et al., 1998). Previous reconnaissance maps (Burg et al., 1998; Liu and Zhong, 1997; Zhang et al., 1992; Ding et al., 2001) differ significantly from one another and from our map, which has been made using our new field observations and parts of the map of the Moutou area by Geng et al. (2006). The

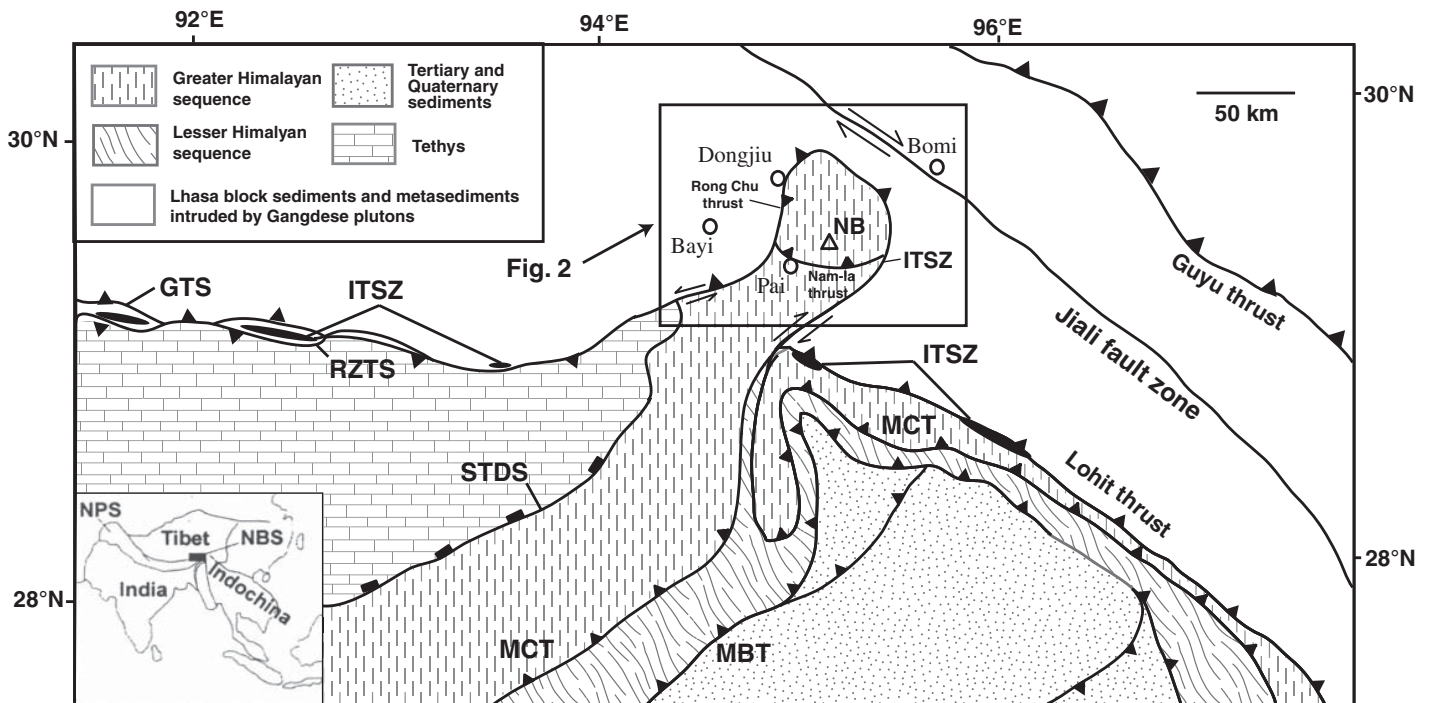


Figure 1. Tectonic sketch map of southeastern Tibet, modified after Ding et al. (2001). Location of Figure 2 shown in box. GTS—Gangdese thrust system, RZTS—Renbu Zedong thrust system, STDS—South Tibetan detachment system, ITSZ—Indus Tsangpo suture zone, MCT—Main Central thrust, MBT—Main Boundary thrust, NB—Namche Barwa. Regional geographic location of Namche Barwa shown in inset. NBS—Namche Barwa syntaxis, NPS—Nanga Parbat syntaxis.

antiform plunges increasingly steeply toward its northern termination, and deforms older, large-scale structural boundaries of the Himalayan orogen, specifically the Indus Tsangpo suture zone, South Tibetan detachment system (STDS), Gangdese thrust system (GTS), and perhaps the Renbu Zedong thrust system (RZTS; see Fig. 1). The margins of the structure are locally modified by active faults—the Rong Chu Fault (a high-angle thrust) along the northern part of the western margin, and the faults passing near Medog (most likely thrusts with right-lateral slip components) on the eastern and southeastern side. We interpret ductile shear zones located along the margins of and within the Namche Barwa antiform as mostly attributable to older Himalayan events, with the main exception to this being the Nam-la ductile shear and fault zone (first recognized by Liu and Zhong, 1997) that crosses the massif south of the peak of Namche Barwa and swings north to connect with the Rong Chu thrust on the western margin. This structure has a significant metamorphic grade contrast across it, expressed in the core gneisses, as discussed below.

Petrology and Granite Genesis

Namche Barwa gneisses south of the Nam-la thrust system are characterized by staurolite + kyanite + plagioclase + biotite + muscovite ± sillimanite and garnet + amphibole + plagioclase assemblages. North of the Nam-la thrust zone, low- to medium-pressure granulite-grade rocks contain garnet + sillimanite + K-feldspar + plagioclase + biotite + quartz ± spinel ± cordierite ± orthopyroxene assemblages (Liu and Zhong, 1997). Thermobarometric studies (Zhong and Ding, 1996; Liu and Zhong, 1997) indicate that rocks of the eastern Himalayan syntaxis experienced at least two metamorphic episodes, the first at high pressures and temperatures (14–15 kbar and ~800 °C), and the second by near-isothermal decompression to 8–10 kbar. High-pressure mafic granulites also occur as relics within these granulite facies rocks (Liu and Zhong, 1997).

In the core of the Namche Barwa massif, granitic dikes and sills intrude Indian basement gneisses on a range of scales. Burg et al. (1998) and Zhang et al. (1992) report leucogranite and pegmatite dikes in the Namche Barwa syntaxis, including leucosomes that crosscut metamorphic layering in the pelitic gneisses. This relationship indicates that anatexis outlasted the main fabric development in the core of Namche Barwa. Single-crystal U-Th-Pb analyses of zircon, xenotime and thorite by Burg et al. (1998) provide leucosome crystallization

ages ranging between 2.9 and 3.9 Ma, and a protolith age of 484 ± 3 Ma. Ding et al. (2001) report U-Pb zircon ages as young as ca. 11 Ma from mafic granulites and two-mica-bearing leucosomes within the core of the massif. The youngest zircon ages (11–25 Ma) are attributed to a later, high-grade metamorphic event, possibly related to decompression melting during rapid exhumation. Granitoids from Namche Barwa with U-Pb zircon ages as young as 3–10 Ma have also been reported by Booth et al. (2004). Trace-element geochemical modeling indicates that these granites were derived from fluid-absent melting of pelites during rapid decompression (Booth et al., 2004).

Cooling History

Ar-Ar, fission-track, and (U-Th)-He ages indicate that the Namche Barwa massif was rapidly exhumed over the past 5 Myr (Burg et al., 1998; Malloy, 2004). The exhumation has been attributed to intense erosion by the Yarlung Tsangpo (~10 mm/yr), coeval with either crustal-scale folding (Burg et al., 1998) or local feedbacks between tectonic and surface processes (Zeitler et al., 2001a). Exhumation appears to be concentrated near the major knickpoint of the river, where riverbed elevations drop 2000 m and maximum local relief is developed. Zircon (U-Th)-He ages range from 0.3 ± 0.1 Ma near this knickpoint to over 50 Ma at distal and higher elevation locations (Malloy, 2004; Zeitler et al., 2006). The young ages extend across mapped structures and appear to define a regional-scale, partial-retention zone with an inflection at ~3000 m of elevation and 1–2 Ma in age (Malloy, 2004). This age distribution suggests at least several kilometers of erosion within the past few million years. Apatite fission-track ages reported from samples within the Namche Barwa massif range from 0.5 ± 0.4 Ma to 8.2 ± 1.6 (Burg et al., 1998) and zircon fission-track ages are ca. 2.5 ± 0.4 Ma (Burg et al., 1998). These two systems have closure temperatures of ~100 °C (apatite) and ~200 °C (zircon), and indicate rapid cooling and exhumation during the past 3 Myr of 100 °C/Myr or more.

Ar-Ar biotite ages are consistently younger than 5 Ma inside the Namche Barwa massif, with the youngest ages (<2 Ma) located around the Tsangpo knickpoint (Malloy, 2004). Previously reported K-Ar mica ages range from 1.2 to 14 Ma within the core gneisses (Zhang et al., 1981; Ratschbacher et al., 1992) and are roughly consistent with our data. Ding et al. (2001) report an Ar-Ar hornblende age of ca. 8 Ma from Namche Barwa, also suggesting rapid cooling and exhumation since at least the late Miocene.

SAMPLES AND ANALYTICAL TECHNIQUES

Petrography and Thermobarometry

Metamorphic and granitic rock samples were collected from the Namche Barwa–Gyala Peri massif and surrounding area, crossing structural boundaries where possible. The location of samples analyzed for thermobarometry are displayed on Figure 2, in the context of the large-scale geology and structures of the area. Approximately 100 thin sections were examined using a petrographic microscope, and characteristic mineral assemblages were determined; these are shown in Figure 3 and summarized in Table 1.

Probe-polished thin sections were made from samples containing appropriate assemblages for thermobarometry. Mineral chemistry was determined with a JEOL 733A electron microprobe at Stanford University with an accelerating voltage of 15 kV and beam current of 15 nA, using natural minerals as standards. In all cases, several mineral pairs were analyzed for each sample. Raw counts were collected for 20 s and converted to oxide wt% by the CITZAF correction procedure. Compositional data for all minerals are tabulated in Item DR1.¹

Prior to thermobarometric calculations, garnets were compositionally traversed at ~20-micron spacings to quantitatively evaluate zoning patterns (Fig. 4; Item DR1 [see footnote 1]), as garnets commonly show zoning that reflects growth events or diffusional modification (e.g., Spear, 1993; Spear and Kohn, 1996; Azor et al., 1997; Kohn et al., 1997; Catlos et al., 2001). Compositional data for garnet traverses are tabulated in Item DR1. Representative profiles of major elements (Mn, Mg, Fe, and Ca) across garnet are shown in Figure 4. These plots allowed us to identify regions of the garnets that are lowest in Mn and Fe/(Fe + Mg), the most suitable for estimating minimum P-T conditions (e.g., Spear and Peacock, 1989). For high-Fe garnets, we back calculated the compositions of matrix biotite, accounting for Fe and Mg added by garnet dissolution during retrograde net-transfer reactions (Kohn and Spear, 2000).

Mineral end-member activities were calculated using the program AX (Holland and Powell, 1998). P-T calculations were performed

¹GSA Data Repository Item 2008211, consisting of Table DR1 (mineral compositions obtained from electron microprobe analyses, used for thermobarometry), Table DR2 (garnet compositions from electron microprobe traverses across garnets), and File DR1 (calculations of garnet dissolution), is available at www.geosociety.org/pubs/ft2008.htm. Requests may also be sent to editing@geosociety.org.

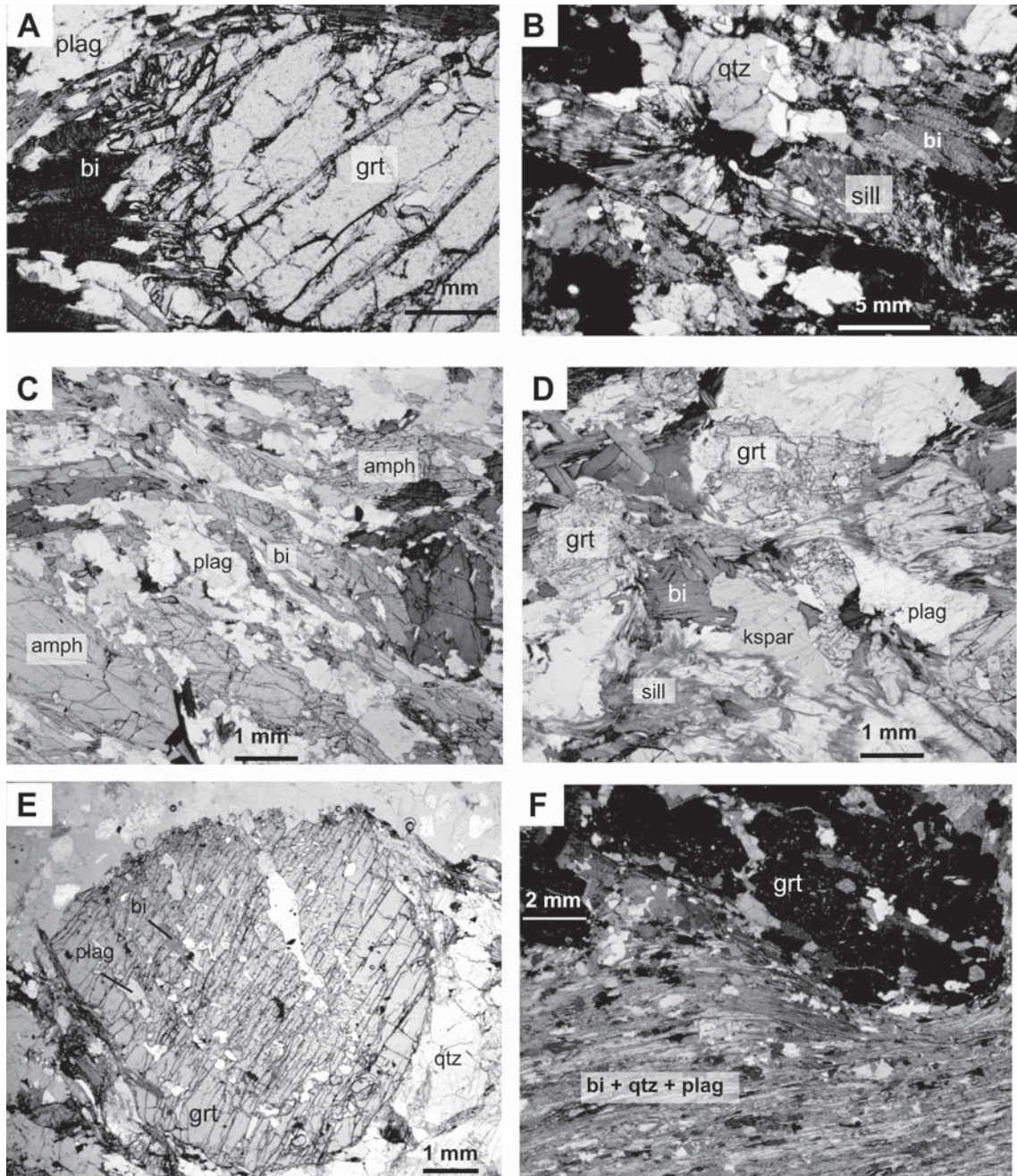


Figure 3. Photomicrographs of representative assemblages: (A) IG-7-01, plane polarized light; (B) IG-1E-01, sillimanite pseudomorph of kyanite, crossed polars; (C) MIII(01)b-288, showing blue-green amphiboles, plane polarized light; (D) GP-3-04, plane polarized light; (E) GP-11-04, plane polarized light; (F) NB-02-05, crossed polars.

TABLE 1. PRESSURE-TEMPERATURE ESTIMATES AND MINERAL ASSEMBLAGES

Sample	Mineral assemblage	Pressure (kbar) and temperature (°C) data
IG-1A-01	qtz, gt, bio, plag	13.8, 850
IG-1E-01	qtz, gt, bio, plag, ksp, ky, sill, il, rt	11.4, 830
IG-2A-01	qtz, gt, bio, hbl, plag, cpx	13.2, 880
IG-7-01	qtz, gt, bio, plag, ksp	11.5, 850
IG-11-01	qtz, gt, bio, plag	12.8, 860
BT-2-01	qtz, gt, bio, hbl, plag, cpx, il	12.5, 750
BT-13-01	qtz, gt, bio, plag, ksp, ms	5.6, 700
M(00)gs-149	qtz, gt, bio, plag	9.6, 680
M(00)gs-15	qtz, gt, bio, hbl, plag, opx, il	8.0, 740
MIII-232	qtz, gt, bio, plag	12.3, 900
MIII-233	qtz, gt, bio, plag	12.7, 690
MIII-236	qtz, gt, bio, plag	11.4, 810
MIII-237	qtz, gt, bio, plag, ep, all	11.6, 900
MV-22	qtz, gt, bio, plag	7.5, 830
NB-02-05	qtz, gt, bio, plag, sill	6.8, 620
NB-02-134	qtz, gt, bio, plag, ksp	10.8, 840
NB-02-142B	qtz, gt, bio, plag, ms	2.8, 460
NB-02-146B	qtz, gt, bio, plag	4.1, 630
NB-02-155B	qtz, gt, st, bio, ky, plag, il	10.8, 700
NB-02-15A	qtz, gt, bio, plag, amph	10.7, 650
NB-02-21B	qtz, gt, bio, plag	4.8, 610
NB-02-31A	qtz, gt, bio, plag	8.1, 720
NB-02-40	qtz, gt, bio, plag, ep	12.0, 790
NB-02-60B	qtz, gt, bio, plag, pyr	10.8, 810
NB-02-78B	qtz, gt, bio, plag, rt, ky	9.2, 670
NB-02-99A	qtz, gt, bio, plag, chl, sill	7.7, 690
GP-2-04	qtz, gt, bio, plag, ksp	7.4, 720
GP-3-04	qtz, gt, bio, plag, sill, py, rt	10.3, 790
GP-4-04	qtz, gt, bio, plag, ksp, sill, py	8.3, 800 (core); 3.5, 670 (rim)
GP-5-04	qtz, gt, bio, plag, ksp	6.3, 620
GP-11-04	qtz, gt, bio, plag, amph	9.1, 770
NB-2-04C	qtz, gt, bio, plag, ksp, il	11.7, 800
NB-2-04E	qtz, gt, bio, plag, sill, chl, il	7.4, 810
NB-7-04A	qtz, gt, bio, plag, ksp	11.4, 850
NB-8-04A	qtz, gt, bio, plag, ksp, sill, il	8.8, 880
NB-10-04A	qtz, gt, bio, plag, ksp, sill	4.8, 730
NB-16-04A	qtz, gt, bio, plag, il	9.2, 710

Note: Mineral assemblages observed in each sample and pressure-temperature estimates obtained using THERMOCALC. Pressures (kbar) and temperatures (°C) represent the average of 1–5 measurements of peak metamorphic conditions (see text for details), and correspond to those plotted on Figure 2. Sample GP-4 lists pressure-temperature estimates using garnet core/rim compositions and inclusion thermobarometry on plagioclase and biotite; these are combined with in-situ monazite ages to determine pressure-temperature changes over time.

Abbreviations: qtz—quartz; gt—garnet; bio—biotite; plag—plagioclase; ksp—k-feldspar; ky—kyanite; sill—sillimanite; hbl—hornblende; cpx—clinopyroxene; opx—orthopyroxene; il—ilmenite; ms—muscovite; rt—rutile; ep—epidote; chl—chlorite; py—pyrite.

using THERMOCALC version 3.1 (Powell and Holland, 1988) with the 1998 thermodynamic data set (Holland and Powell, 1998). We employed the average P-T approach of Powell and Holland (1994) for the observed assemblages, involving several linearly independent reactions in the K_2O -FeO-MgO-Al₂O₃-SiO₂-H₂O (KFMASH) system. A fluid composition of $X_{H_2O} = 1.0$ was assumed for all sample calculations. Peak metamorphic conditions were calculated using inner rim compositions of garnet (i.e., those not affected by late diffusional exchange; Spear, 1991; Spear and Florence, 1992) paired with matrix biotite and plagioclase. Most of the garnet cores exhibit flat compositional profiles (Fig. 4) and are characteristic of garnets that have been homogenized at high metamorphic conditions (Tuccillo et al., 1990; Spear, 1993). Rims typically show sharp enrichment of Mn, inferred

to represent substantial resorption. Concomitant decreases in Ca and Mg/(Fe + Mg) indicate that resorption resulted from net transfer reactions involving garnet consumption and plagioclase growth during decompression and cooling. These retrograde net transfer reactions can significantly affect the generated P-T results (Selverstone and Chamberlain, 1990; Spear, 1991; Spear and Florence, 1992; Kohn and Spear, 2000). To assess the impact of retrograde net transfer reactions (e.g., Kohn and Spear, 2000), thermobarometric estimates were made using compositions of matrix plagioclase and biotite both near and far from the garnet. Variations in the calculated pressures and temperatures were minimal. As such, peak metamorphic conditions (see Fig. 2) were derived from garnet compositions just inside the resorption-induced rim (the Mn and Fe/(Fe + Mg) trough) and from matrix plagioclase

and biotite. These pressures and temperatures are compatible with the observed assemblages (Table 1); however, in some cases it is possible that calculated temperatures were slightly overestimated due to retrograde garnet dissolution and Fe-Mg exchange with biotite (i.e., Kohn and Spear, 2000). To quantify this effect, we calculated the amount of dissolved garnet following the method of Kohn and Spear (2000). These calculations are tabulated in Item DR1 (see footnote 1), and indicate that the volumes of dissolved garnet are small (<5%). However, accounting for Fe and Mg added to biotite by garnet dissolution yields temperatures that, for some samples, are as much as 50–100 °C lower than originally calculated. Therefore we incorporated these calculations into the final temperatures and pressures reported in Table 1.

Geochronology

Monazite and titanite U-Th-Pb analyses were conducted at Stanford University using the sensitive high-resolution ion microprobe–reverse geometry (SHRIMP-RG) co-operated by the U.S. Geological Survey and Stanford University. Separated-grain and in-situ techniques were utilized for this study. Minerals were separated using standard procedures of crushing, grinding, and heavy liquid and magnetic separation. Zircon and monazite grains were mounted in epoxy and polished to approximately half their mean thickness, then characterized using backscattered electron imaging (BSE) to illuminate internal zoning. Further chemical characterization of monazite was achieved through X-ray mapping using a scanning electron microscope. In-situ ages (samples GP4-11a, GP4-11b, GP4-11c, GP4-2, and GP4-18; see Table 2) were obtained on monazite included in garnet. For these analyses, garnets were separated from the rock, mounted into 1-inch epoxy, ion-microprobe mounts, and monazite inclusions within were dated. For U-Th-Pb SHRIMP analysis, the mounts were coated with gold, and each sample was sputtered with a primary beam of O⁻ ions using a spot size of ~25 μm. This spot size was used during in-situ analysis as well, although the monazite grains were typically much smaller than 25 μm. For monazite, counts of CePO₂, ThNdO₂, ²⁰⁴Pb, background, ²⁰⁶Pb, ²⁰⁷Pb, ²⁰⁸Pb, ²³²Th, ²³⁸U, ²⁴⁸ThO, and ²⁵⁴UO were measured from the secondary beam. For titanite, CaTi₂O₄, ²⁰⁴Pb, background, ²⁰⁶Pb, ²⁰⁷Pb, ²⁰⁸Pb, ²³²Th, ²³⁸U, ²⁴⁸ThO, and ²⁵⁴UO were measured. Analytical and data-reduction procedures followed those given in Williams (1998) and Ireland and Williams (2003). Concentration and age data for monazites use standard 44069 with an age of

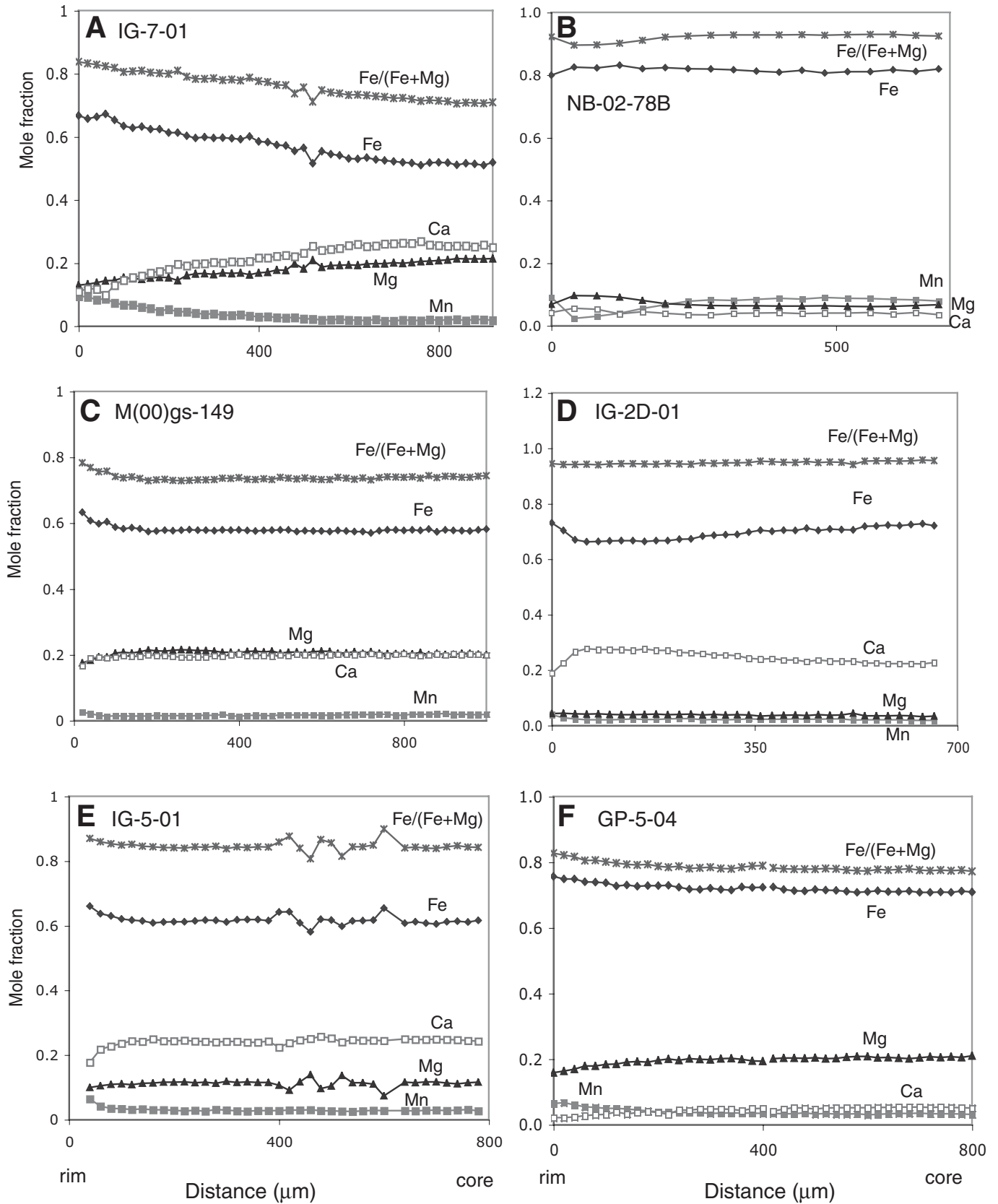


Figure 4. Garnet major-element profiles, showing relatively flat core compositional zoning, suggesting homogenization at high metamorphic grade. Weak, bell-shaped profile in (A) reflects prograde garnet growth during earlier metamorphism. Near-rim modification of Ca, Mn, and Fe/(Fe + Mg) in garnets (B)–(E) is due to garnet resorption during retrograde net-transfer reactions.

TABLE 2. U-Th-Pb ISOTOPIC DATA

Spot name	Common ²⁰⁶ Pb (%)	U (ppm)	Th (ppm)	²³² Th/ ²³⁸ U	²⁰⁶ Pb/ ²³⁸ U Age (Ma ± 1σ)	Total ²³⁸ U/ ²⁰⁶ Pb (± % error)	Total ²³⁵ U/ ²⁰⁶ Pb (± % error)	Total ²⁰⁸ Pb/ ²³² Th (± % error)	²⁰⁸ Pb/ ²³² Th age (Ma ± 1σ)
BT8-01 monazite									
BT8-1.1	0.04	3155	20,505	6.72	207.1 ± 1.7	30.6 ± 0.8	0.0507 ± 0.6	0.01062 ± 2.3	213.5 ± 2.8
BT8-2.1	-0.08	2364	11,255	4.92	229.8 ± 1.9	27.6 ± 0.8	0.0505 ± 0.5	0.01134 ± 0.9	228.2 ± 2.0
BT8-2.2	-0.04	2470	27,126	11.35	69.9 ± 0.7	91.5 ± 0.9	0.0491 ± 0.9	0.00344 ± 1.1	69.4 ± 0.7
BT-8-3.1	0.11	4109	22,376	5.63	60.6 ± 0.5	105.5 ± 0.9	0.0500 ± 0.7	0.00296 ± 1.3	59.6 ± 0.7
BT-8-4.1	-0.12	1473	4082	2.86	225.8 ± 2.0	28.0 ± 0.9	0.0508 ± 0.6	0.01124 ± 1.1	226.5 ± 2.3
BT-8-4.2	-0.04	4878	24,505	5.19	60.1 ± 0.5	106.5 ± 0.9	0.0489 ± 0.8	0.00258 ± 1.0	52.2 ± 0.5
BT-8-5.1	0.08	4057	23,002	5.86	67.1 ± 0.6	95.5 ± 0.9	0.0480 ± 0.8	0.00330 ± 1.0	66.5 ± 0.6
BT8-6.1	-0.04	3296	26,599	8.34	66.3 ± 0.6	96.6 ± 0.9	0.0489 ± 0.8	0.00324 ± 1.0	65.4 ± 0.6
BT8-7.1	0.05	3921	21,295	5.61	114.1 ± 1.0	55.9 ± 0.8	0.0490 ± 0.6	0.00551 ± 1.0	111.1 ± 1.0
BT8-8.1	0.01	1401	37,711	27.81	1069.3 ± 9.4	5.4 ± 0.9	0.0910 ± 0.2	0.05739 ± 1.1	1127.9 ± 11.7
BT8-8.2	-0.13	2587	22,796	9.11	55.4 ± 0.5	115.4 ± 0.9	0.0494 ± 1.0	0.00255 ± 1.1	51.6 ± 0.5
BT8-9.1	0.12	1811	19,936	11.38	222.2 ± 1.9	28.5 ± 0.9	0.0518 ± 0.6	0.01104 ± 1.0	221.7 ± 2.0
BT8-10.1	0.12	5177	34,476	6.88	68.7 ± 0.6	93.2 ± 0.8	0.0485 ± 0.7	0.00336 ± 0.9	67.6 ± 0.6
BT8-11.1	0.12	1672	12,421	7.68	199.6 ± 1.7	31.7 ± 0.9	0.0521 ± 0.7	0.00948 ± 3.1	190.6 ± 4.3
BT8-12.1	-0.14	3461	28,357	8.46	68.1 ± 0.6	94.0 ± 0.9	0.0483 ± 0.8	0.00328 ± 1.0	66.3 ± 0.6
BT8-13.1	-0.06	2599	17,025	6.77	215.2 ± 1.8	29.4 ± 0.8	0.0506 ± 0.5	0.01064 ± 0.9	214.0 ± 1.9
BT8-14.1	0.10	3197	26,305	8.50	67.0 ± 0.6	95.4 ± 0.9	0.0498 ± 0.8	0.00333 ± 1.7	67.2 ± 0.9
BT8-15.1	-0.01	2723	17,459	6.63	216.0 ± 1.8	29.3 ± 0.9	0.0510 ± 0.5	0.01065 ± 1.0	214.2 ± 2.0
BT8-16.1	0.20	3914	20,987	5.54	57.3 ± 0.5	111.8 ± 0.9	0.0488 ± 0.8	0.00286 ± 1.0	57.5 ± 0.6
BT13-01 monazite									
BT13-1.1	0.35	1154	16,783	15.03	62.0 ± 0.4	102.8 ± 0.7	0.0526 ± 1.4	0.00300 ± 1.0	60.5 ± 0.6
BT13-2.1	-0.20	803	16,955	21.82	62.5 ± 0.5	102.0 ± 0.9	0.0523 ± 1.7	0.00310 ± 1.5	62.6 ± 0.7
BT13-1.2	-0.21	1067	13,514	13.08	46.6 ± 0.4	136.8 ± 0.9	0.0528 ± 1.8	0.00227 ± 1.3	45.8 ± 0.6
BT13-3.1	0.84	355	23,024	66.97	53.7 ± 0.8	116.2 ± 1.4	0.0690 ± 2.5	0.00254 ± 1.8	51.2 ± 0.9
BT13-4.1	0.10	776	20,125	26.80	27.5 ± 0.3	228.8 ± 1.2	0.0650 ± 2.4	0.00132 ± 1.8	26.7 ± 0.5
BT13-5.1	-0.73	951	20,051	21.78	51.7 ± 0.5	123.3 ± 0.9	0.0538 ± 1.8	0.00242 ± 1.2	49.0 ± 0.6
BT13-6.1	0.36	1509	14,929	10.22	67.2 ± 0.4	94.6 ± 0.6	0.0550 ± 1.2	0.00328 ± 0.9	65.9 ± 0.6
BT13-6.2	-1.54	724	20,967	29.90	42.9 ± 0.5	147.4 ± 1.1	0.0595 ± 2.2	0.00190 ± 1.5	38.6 ± 0.6
BT13-7.1	0.44	711	24,325	35.34	49.4 ± 0.5	128.4 ± 1.0	0.0567 ± 2.0	0.00226 ± 1.5	45.5 ± 0.7
BT13-8.1	0.11	621	18,118	30.17	27.1 ± 0.4	228.3 ± 1.3	0.0778 ± 2.4	0.00132 ± 1.9	26.7 ± 0.5
BT13-9.1	-0.57	1116	16,345	15.14	58.4 ± 0.5	109.2 ± 0.8	0.0522 ± 1.7	0.00287 ± 1.1	58.0 ± 0.6
BT13-10.1	0.11	393	25,499	66.97	51.9 ± 0.7	121.2 ± 1.3	0.0638 ± 2.5	0.00243 ± 1.8	49.1 ± 0.9
GP2-04 monazite									
GP2-1.1	0.82	7792	52,362	6.94	5.9 ± 0.1	1084.9 ± 0.9	0.0526 ± 2.4	0.00028 ± 1.5	5.4 ± 0.1
GP2-2.1	0.95	5750	45,800	8.23	6.1 ± 0.0	1045.3 ± 0.7	0.0536 ± 2.5	0.00029 ± 1.1	5.8 ± 0.1
GP2-2.2	1.08	5378	37,433	7.19	6.1 ± 0.0	1041.4 ± 0.7	0.0547 ± 2.6	0.00028 ± 1.2	5.9 ± 1.5
GP2-3.1	-0.19	4145	39,534	9.86	6.9 ± 0.1	933.2 ± 0.8	0.0447 ± 3.1	0.00025 ± 1.5	5.1 ± 0.1
GP2-4.1	0.80	6433	59,653	9.58	6.1 ± 0.0	1050.1 ± 0.7	0.0525 ± 2.4	0.00028 ± 1.2	5.6 ± 0.1
GP2-5.1	0.61	5185	37,744	7.52	4.9 ± 0.0	1298.7 ± 0.8	0.0510 ± 3.0	0.00022 ± 1.6	4.5 ± 0.1
GP2-6.1	1.07	4110	42,804	10.76	5.7 ± 0.1	1110.9 ± 0.8	0.0546 ± 3.1	0.00024 ± 1.4	4.9 ± 0.1
GP2-7.1	1.16	6930	59,595	8.89	6.0 ± 0.0	1064.7 ± 0.6	0.0553 ± 2.3	0.00028 ± 1.0	5.6 ± 0.1
GP2-7.2	-0.31	5509	42,637	8.00	7.2 ± 0.0	901.7 ± 0.7	0.0437 ± 2.7	0.00026 ± 1.2	5.4 ± 0.1
GP2-8.1	1.26	6405	50,192	8.10	6.1 ± 0.0	1042.0 ± 0.8	0.0561 ± 2.4	0.00028 ± 1.2	5.8 ± 0.1
GP2-9.1	-0.60	4876	38,315	8.12	7.3 ± 0.0	882.7 ± 0.7	0.0415 ± 2.7	0.00026 ± 1.2	5.3 ± 0.1
GP2-10.1	-0.45	4777	36,965	8.00	6.8 ± 0.0	955.7 ± 0.7	0.0426 ± 2.7	0.00025 ± 1.4	4.8 ± 0.1
GP3-04 monazite									
GP3-1.1	6.25	3322	38,459	11.96	3.9 ± 0.1	1543.4 ± 1.1	0.0954 ± 3.1	0.00012 ± 1.7	2.5 ± 0.0
GP3-2.1	9.55	3688	40,565	11.36	6.8 ± 0.1	852.0 ± 0.8	0.1216 ± 1.9	0.00027 ± 1.5	5.0 ± 0.1
GP3-3.1	9.09	3195	41,229	13.33	7.4 ± 0.1	790.9 ± 0.8	0.1180 ± 2.0	0.00024 ± 1.3	4.3 ± 0.1
GP3-4.1	7.90	4849	49,553	10.56	7.9 ± 0.1	753.8 ± 0.6	0.1086 ± 1.7	0.00027 ± 1.1	4.9 ± 0.1
GP3-5.1	7.57	4556	44,477	10.09	8.6 ± 0.1	692.2 ± 0.6	0.1060 ± 1.7	0.00033 ± 1.2	6.3 ± 0.1
GP3-6.1	9.08	4358	42,239	10.01	7.6 ± 0.1	774.2 ± 0.7	0.1179 ± 1.8	0.00030 ± 1.1	5.5 ± 0.1
GP3-7.1	8.08	4487	51,627	11.89	8.1 ± 0.1	733.4 ± 0.7	0.1100 ± 1.8	0.00027 ± 1.1	5.0 ± 0.1
GP3-8.1	8.76	4114	45,592	11.45	7.9 ± 0.1	746.8 ± 0.7	0.1154 ± 1.8	0.00030 ± 1.2	5.4 ± 0.1
GP3-9.1	8.42	4223	43,537	10.65	8.1 ± 0.1	732.5 ± 0.7	0.1127 ± 1.8	0.00030 ± 1.3	5.6 ± 0.1
GP3-10.1	8.59	3529	44,151	12.93	8.1 ± 0.1	723.8 ± 0.7	0.1140 ± 1.9	0.00026 ± 1.2	4.9 ± 0.1
GP3-11.1	9.41	3786	46,835	12.78	8.0 ± 0.1	725.7 ± 0.7	0.1205 ± 1.9	0.00027 ± 1.2	5.0 ± 0.1
GP3-12.1	7.43	6588	45,052	7.07	7.1 ± 0.1	845.6 ± 0.7	0.1048 ± 1.6	0.00035 ± 1.0	6.6 ± 0.1
GP4-04 monazite									
GP4-1.1	3.52	8652	44,214	5.28	9.4 ± 0.1	658.0 ± 0.4	0.0740 ± 1.3	0.00043 ± 0.8	8.2 ± 0.1
GP4-2.1	4.16	7523	49,695	6.83	9.2 ± 0.1	670.6 ± 0.5	0.0791 ± 1.4	0.00042 ± 0.8	8.2 ± 0.1
GP4-2.2	6.61	6298	49,488	8.12	7.3 ± 0.1	818.9 ± 0.6	0.0984 ± 1.6	0.00032 ± 1.1	6.0 ± 0.1
GP4-3.1	4.12	4790	42,665	9.20	5.5 ± 0.1	1128.8 ± 0.9	0.0787 ± 2.4	0.00022 ± 1.5	4.1 ± 0.1
GP4-4.1	3.91	9135	44,972	5.09	9.3 ± 0.1	665.7 ± 0.4	0.0771 ± 1.3	0.00044 ± 0.8	8.3 ± 0.1
GP4-5.1	5.65	3398	40,092	12.19	6.7 ± 0.1	911.7 ± 0.8	0.0908 ± 2.3	0.00030 ± 1.3	5.8 ± 0.1
GP4-6.1	3.37	5287	40,743	7.96	8.3 ± 0.1	751.3 ± 0.6	0.0729 ± 1.9	0.00034 ± 1.0	6.7 ± 0.1
GP4-7.1	3.14	5371	42,003	8.08	9.8 ± 0.1	637.2 ± 0.5	0.0711 ± 1.8	0.00039 ± 1.0	7.7 ± 0.1
GP4-8.1	4.54	7691	47,608	6.40	9.6 ± 0.1	642.5 ± 0.5	0.0821 ± 1.4	0.00046 ± 0.8	9.0 ± 0.1
GP4-9.1	4.34	6300	32,849	5.39	9.1 ± 0.1	680.9 ± 0.5	0.0805 ± 1.6	0.00045 ± 1.0	8.8 ± 0.1
GP4-10.1	2.72	4859	9745	2.07	9.4 ± 0.1	665.4 ± 0.6	0.0677 ± 1.9	0.00051 ± 1.2	9.8 ± 0.2
GP4-11.1	4.70	10757	60,673	5.83	8.9 ± 0.1	687.5 ± 0.4	0.0833 ± 1.3	0.00043 ± 0.8	8.3 ± 0.1
GP4-04 monazite <i>in situ</i>									
GP4-11a	5.68	8166	52,999	6.7	7.2 ± 0.2	847.4 ± 2.8	0.0910 ± 8.3	0.00032 ± 5.0	6.4 ± 0.3
GP4-11b	5.72	7987	45,970	5.9	8.3 ± 0.2	730.9 ± 2.2	0.0914 ± 6.8	0.00041 ± 4.9	7.9 ± 0.4

(continued)

TABLE 2. U-Th-Pb ISOTOPIC DATA

Spot name	Common ²⁰⁶ Pb (%)	U (ppm)	Th (ppm)	²³² Th/ ²³⁸ U	²⁰⁶ Pb/ ²³⁸ U Age (Ma ± 1σ)	Total ²³⁸ U/ ²³⁶ Pb (± % error)	Total ²⁰⁷ Pb/ ²³⁵ Pb (± % error)	Total ²⁰⁸ Pb/ ²³² Th (± % error)	²⁰⁸ Pb/ ²³² Th age (Ma ± 1σ)
GP4-11e	2.93	11,055	53,382	5.0	9.2 ± 0.3	679.2 ± 2.7	0.0693 ± 9.0	0.00051 ± 5.2	9.5 ± 0.6
GP4-2	9.44	5530	33,219	6.2	10.4 ± 0.1	558.4 ± 0.7	0.1208 ± 2.1	0.00062 ± 1.1	11.3 ± 0.2
GP4-18	5.76	4483	31,433	7.2	9.6 ± 0.1	634.0 ± 0.9	0.0917 ± 2.7	0.00055 ± 1.4	10.6 ± 0.2
NB1-04 monazite									
NB1-1.1	4.55	6952	37,559	5.58	8.7 ± 0.1	703.9 ± 0.5	0.0822 ± 1.5	0.00044 ± 0.9	8.3 ± 0.1
NB1-2.1	12.11	2237	52,604	24.30	5.3 ± 0.1	1063.1 ± 1.2	0.1418 ± 2.8	0.00024 ± 1.8	4.6 ± 0.1
NB1-2.2	12.31	2890	44,471	15.90	3.7 ± 0.1	1529.3 ± 1.2	0.1434 ± 2.8	0.00020 ± 1.8	3.9 ± 0.1
NB1-3.1	3.58	6569	42,542	6.69	8.8 ± 0.1	707.9 ± 0.5	0.0745 ± 1.6	0.00041 ± 1.0	7.8 ± 0.1
NB1-3.2	3.81	6265	42,192	6.96	9.4 ± 0.1	656.3 ± 0.5	0.0763 ± 1.7	0.00042 ± 1.0	8.1 ± 0.1
NB1-04 titanite									
NB1sph-1.1	93.83	6.44	2	0.27	28.1 ± 56.4	14.1 ± 4.38	0.7908 ± 3.7		
NB1sph-2.1	81.63	82.19	79	1.00	7.9 ± 4.7	149.2 ± 2.46	0.6912 ± 3.5		
NB1sph-3.1	87.89	11.78	4	0.38	36.9 ± 35.6	21.1 ± 3.99	0.7435 ± 4.0		
NB1sph-4.1	94.44	37.31	10	0.27	4.4 ± 10.0	81.6 ± 3.28	0.7924 ± 4.3		
NB2c-04 titanite									
NB2c-1.1	71.88	190.33	211	1.14	10.2 ± 3.4	177.5 ± 1.74	0.6142 ± 2.6		
NB2c-2.1	68.31	167.60	228	1.40	12.7 ± 3.6	160.3 ± 1.80	0.5861 ± 2.7		
NB2c-3.1	73.72	414.40	358	0.89	3.5 ± 1.3	490.3 ± 1.93	0.6283 ± 3.0		
NB2c-4.1	85.02	208.23	189	0.94	3.2 ± 2.4	299.2 ± 2.11	0.7176 ± 3.4		
NB2c-5.1	65.87	174.99	295	1.74	15.5 ± 3.9	141.5 ± 1.56	0.5670 ± 2.3		
NB2c-6.1	80.42	308.33	177	0.59	3.6 ± 1.9	347.2 ± 1.79	0.6813 ± 2.7		
NB2c-7.1	77.67	233.97	251	1.11	5.8 ± 2.6	250.2 ± 1.78	0.6597 ± 2.7		
NB2c-8.1	78.95	194.18	188	1.00	5.3 ± 2.6	255.0 ± 1.91	0.6698 ± 2.8		
NB2c-9.1	88.04	107.92	162	1.55	9.2 ± 8.7	83.6 ± 1.69	0.7421 ± 2.2		
NB2c-10.1	75.06	285.07	137	0.50	4.8 ± 1.9	331.7 ± 1.75	0.6390 ± 2.7		
GP7-04 titanite									
GP7-1.1	71.12	47.25	150	3.28	20.0 ± 6.5	93.1 ± 2.61	0.6088 ± 3.6		
GP7-2.1	75.85	49.80	72	1.49	22.0 ± 9.0	70.7 ± 2.30	0.6464 ± 3.0		
GP7-3.1	78.27	32.98	181	5.69	18.7 ± 8.9	74.7 ± 2.80	0.6654 ± 3.7		
GP7-4.1	71.11	44.91	213	4.91	21.5 ± 7.0	86.3 ± 2.51	0.6088 ± 3.5		
GP7-5.1	50.53	94.84	583	6.35	25.2 ± 3.4	126.1 ± 2.00	0.4462 ± 3.2		
GP7-6.1	78.24	39.92	156	4.05	19.4 ± 9.2	72.1 ± 2.59	0.6652 ± 3.4		
GP7-7.1	64.07	74.21	305	4.25	21.4 ± 5.0	108.2 ± 2.19	0.5531 ± 3.2		
GP7-8.1	70.68	50.02	183	3.78	19.9 ± 6.3	94.7 ± 2.85	0.6053 ± 3.4		
GP7-9.1	67.43	71.45	249	3.60	18.2 ± 5.1	115.3 ± 2.79	0.5795 ± 4.2		
GP7-10.1	80.41	36.59	133	3.74	18.0 ± 9.8	70.0 ± 2.72	0.6822 ± 3.5		
GP7-11.1	81.40	27.91	87	3.22	20.2 ± 11.7	59.4 ± 3.04	0.6903 ± 3.9		
GP7-12.1	88.14	20.86	77	3.81	19.7 ± 19.2	38.7 ± 2.99	0.7439 ± 3.4		
NB13a-04 titanite									
NB-13a-1.1	1.30	503.27	118	0.24	464.7 ± 2.7	13.2 ± 0.52	0.0669 ± 2.9		
NB-13a-2.1	6.67	189.20	48	0.26	53.8 ± 1.0	111.4 ± 1.57	0.0999 ± 5.2		
NB-13a-2.2	0.35	602.52	137	0.23	551.2 ± 2.7	11.2 ± 0.48	0.0614 ± 1.4		
NB-13a-3.1	0.46	550.41	136	0.26	552.0 ± 2.7	11.1 ± 0.49	0.0623 ± 1.0		
NB-13a-4.1	0.34	412.54	97	0.24	533.8 ± 3.1	11.5 ± 0.58	0.0609 ± 1.3		
NB-13a-4.2	45.19	181.60	45	0.26	10.2 ± 1.3	347.7 ± 2.82	0.4033 ± 7.4		
NB-13a-5.1	0.91	427.92	64	0.15	542.1 ± 3.2	11.3 ± 0.59	0.0657 ± 1.3		
NB-13a-6.1	0.30	584.69	163	0.29	565.0 ± 2.7	10.9 ± 0.49	0.0614 ± 1.0		
NB-13a-7.1	0.33	389.76	122	0.32	556.1 ± 3.3	11.1 ± 0.60	0.0614 ± 1.3		
NB-13a-8.1	0.81	164.44	49	0.31	544.7 ± 5.0	11.2 ± 0.93	0.0650 ± 2.0		
NB-13a-8.2	7.59	515.08	159	0.32	209.2 ± 2.7	28.0 ± 0.66	0.1110 ± 3.3		
NB-13a-9.1	10.95	18.73	7	0.38	292.4 ± 11.7	19.2 ± 3.15	0.1401 ± 10.4		
NB-13a-10.1	0.24	444.68	115	0.27	550.0 ± 3.1	11.2 ± 0.56	0.0605 ± 1.2		
NB-13a-11.1	0.33	492.96	114	0.24	547.3 ± 3.0	11.2 ± 0.56	0.0612 ± 1.2		
NB-13a-12.1	1.31	44.36	22	0.50	517.5 ± 9.7	11.8 ± 1.88	0.0683 ± 3.8		
NB-13a-13.1	5.91	16.20	3	0.20	453.9 ± 14.9	12.9 ± 3.16	0.1040 ± 5.8		

424.9 ± 0.4 Ma and average U concentration of 2500 ppm (Aleinikoff et al., 2006), or standard Wendell with an age of 301 Ma and average U concentration of 5500 ppm (Joseph Wooden, 2005, personal commun.). Concentration and age data for titanites are standardized against BLR-1 with an age of 1047 ± 0.4 Ma and average U concentration of 250 ppm (Aleinikoff et al., 2007). All reported ages were determined using the data-reduction programs Squid (Ludwig, 2001) and Isoplot (Ludwig, 2003). Common Pb corrections were made using the two-stage average crustal Pb model of Stacey and Kramers (1975).

RESULTS AND INTERPRETATION

Metamorphic Assemblages

We observed five distinct metamorphic assemblages from rocks in and around Namche Barwa: (1) muscovite-chlorite-bearing metasediments belonging to the Lhasa Block, around the outside of the syntaxial region, (2) amphibolitic mylonites of the Indus-Tsangpo suture, containing blue-green amphiboles, (3) staurolite-kyanite-bearing Tethyan metasediments wrapping around suture zone rocks, (4) sillimanite-potassium feldspar-bearing rocks within Namche

Barwa gneisses, north of the Nam-la thrust, and (5) kyanite-potassium feldspar-bearing gneisses south of the Nam-la thrust. All of these rock types also contain garnet, plagioclase, biotite, and quartz, with minor amounts of ilmenite. Garnets are inclusion-rich and range from 1 to 20 mm in diameter. Inclusion trails in garnets are typically at an angle to the dominant foliation (i.e., Fig. 3A), which is defined by micas and/or quartz ribbons. Sillimanite, where present, occurs either as fibrolitic sprays or as pseudomorphs of kyanite (i.e., Fig. 3B), and appears to be postkinematic with respect to ductile foliation. Garnets typically exhibit decompression

reaction textures, in which garnet rims have broken down to quartz and plagioclase. This is also seen in garnet zoning profiles (Fig. 4), which show an abrupt decrease of Ca content in garnet rims, suggesting that Ca was transported from garnet to plagioclase during retrograde stages of metamorphism.

The boundaries between these metamorphic assemblages appear to be structurally controlled and do not represent true metamorphic isograds. Zones 1–4 are interpreted as distinct tectono-stratigraphic units juxtaposed along major structural boundaries between zones 1, 2, and 3, associated with the Indus Tsangpo suture zone and younger high-strain zones also localized there. Inside the Namche Barwa massif, however, the bulk of metapelitic gneisses are characterized by a garnet-biotite-plagioclase-quartz-potassium feldspar \pm muscovite \pm kyanite \pm sillimanite assemblage. Within these gneisses, sillimanite-bearing rocks occur primarily in the northern part of the antiform, whereas kyanite-bearing rocks are present to the south. The boundary between these two assemblages coincides roughly with the Nam-la thrust system, suggesting that sillimanite-bearing rocks were carried to the surface from greater depth along the Nam-la thrust.

Thermobarometry

Thermobarometric calculations based on the average P-T method are summarized in Table 1 and plotted with sample numbers on Figure 2. Temperatures and pressures calculated from THERMOCALC, incorporating typical uncertainty for each mineral end-member activity and errors in the thermodynamic data set, are at best accurate to ~ 50 °C and ~ 1 kbar. Each P-T point plotted on Figure 2 represents the average of 1–5 individual calculations based on analyses of garnet, biotite, and plagioclase coexisting with aluminosilicate and quartz within a single sample. Although there are large uncertainties associated with thermobarometric calculations, we emphasize that our primary concern is with broad patterns among the P-T data and implications for the evolution of Namche Barwa. Despite the relatively large uncertainties in the P-T calculations, the computed conditions agree with the expected pressure and temperature ranges of the observed metamorphic assemblages (Table 1).

The wide range of calculated P-T conditions allows grouping based on spatial trends. These groups are distinct at the 95% confidence interval. P-T conditions correspond to six geographic zones (see Fig. 2): (1) Lhasa Block metasediments around the outside of the syntaxial region, (2) suture zone amphibolites wrapped around Namche Barwa gneisses, (3) Tethyan

metasediments wrapping around suture zone rocks, (4) the Gyala Peri region north of Namche Barwa, (5) the core of Namche Barwa, close to the Tsangpo Gorge, and (6) south of Namche Barwa, across the Nam-la thrust.

Outside the Namche Barwa syntaxis, medium-grade Lhasa Block metasediments are intruded by plutons associated with Gangdese arc magmatism. These rocks yield P-T conditions of equilibration that are the lowest among our study area (~ 3 – 7 kbar, 500 – 700 °C), and likely reflect regional metamorphism prior to or associated with early India-Asia collision. A band of high-pressure amphibolites (15 – 20 kbar), which is interpreted as a remnant of the Tsangpo suture zone, wraps around the Namche Barwa gneisses. Outside this band is another zone of quartzofeldspathic and metasedimentary gneisses (forming basement and lowest cover of the Lhasa Block), which equilibrated at upper-amphibolite-facies conditions (~ 8 – 12 kbar and ~ 600 – 800 °C). Within the core of Namche Barwa, P-T data from metapelitic rocks indicate that final equilibration occurred at high temperature and pressure (~ 11 – 14 kbar and 800 – 950 °C). This is consistent with the observed K-feldspar-bearing assemblages, as well as with results reported by Liu and Zhong (1997). High P-T conditions suggest that these rocks represent deep exposures of the crust, and indicate that the core of Namche Barwa is the locus of the most deeply exhumed rocks. There is a clear metamorphic break between the core of Namche Barwa and the region south of the Nam-la thrust (Fig. 5), where lower pressures and slightly lower temperatures characterize the assemblages (~ 5 – 9 kbar and 700 – 800 °C). Similarly, north of Namche Barwa in the vicinity of Gyala Peri, four samples (GP-2, GP-3, GP-4, and GP-5) yield pressures and temperatures that are somewhat lower (7 – 10 kbar and ~ 800 – 900 °C), suggesting the presence of metamorphic break between this area north of the Gyala Peri Peak and the Tsangpo Gorge outcrops north of Namche Barwa. However, we believe this structure is likely much older than the Nam-la thrust and related to an early Himalayan event involving emplacement of the higher pressure rocks back into the crust.

Metamorphic Geochronology

Monazite Ages

Monazite (Ce, La, Th)PO₄ is an accessory phase commonly used for U-Pb and Th-Pb dating of crustal rocks. Monazites usually contain $<0.5\%$ U and from 1% to 30% Th (Overstreet, 1967), sustain little radiation damage, and are unlikely to lose Pb even at high-grade metamorphic conditions. There are complications,

however, with assigning monazite ages to specific P-T conditions of formation, due to the large range of conditions over which monazite grows. Monazite forms as a metamorphic mineral under lower amphibolite-facies conditions (Smith and Barreiro, 1990; Kingsbury et al., 1993; Ferry, 2000; Pyle and Spear, 2003; Wing et al., 2003; Kohn and Malloy, 2004) up to granulite facies conditions (Bingen et al., 1996; Bea and Montero, 1999; Pyle et al., 2001; Pyle and Spear, 2003). The appearance of monazite in conjunction with metamorphic index minerals such as aluminosilicate (e.g., Ferry, 2000; Wing et al., 2003), staurolite (e.g., Kohn and Malloy, 2004), or garnet (e.g., Harrison et al., 1997; Foster et al., 2000; Catlos et al. 2001; Kohn et al., 2001) suggests that monazite can potentially date timing of amphibolite-facies metamorphism. However, monazite may form and recrystallize multiple times with subsequent metamorphic episodes, and distinct age or compositional domains are observed in many cases (e.g., Teufel and Heinrich, 1997; Townsend et al., 2001; Kohn et al., 2005). Bingen and van Breemen (1998) suggest that monazite ages may reflect primary or secondary growth linked to metamorphic reactions involving redistribution of rare-earth elements (REEs) and Th. Indeed, age patterns associated with Th and Pb zoning in granulite-facies monazite indicate that monazite may be reset by secondary replacement of the crystal structure rather than by volume diffusion of Pb (DeWolf et al., 1993; Zhu et al., 1997). Interpretation of monazite ages therefore requires knowledge of both the chemical zoning patterns as well as the likely prograde reactions responsible for monazite growth. We consider these factors when discussing metamorphic age significance below.

Both U-Pb and Th-Pb ratios and ages are reported in this study (Table 2). All U-Pb ages are ²⁰⁷Pb-corrected ²⁰⁶Pb/²³⁸U ages, and Th-Pb ages are ²⁰⁴Pb-corrected ²⁰⁸Pb/²³²Th ages. Because monazites can contain several weight percent thorium, significant ²³⁰Th, an intermediate member of the ²³⁸U to ²⁰⁶Pb decay chain, may be incorporated at crystallization. The effect of ²³⁰Th incorporation is production of excess ²⁰⁶Pb that is unsupported by the existing ²³⁸U, resulting in ²⁰⁶Pb/²³⁸U ages that are too old (e.g., Schärer, 1984; Parrish, 1990). A correction technique for excess ²⁰⁶Pb is outlined by Parrish (1990), but it requires knowledge of the whole-rock ²³⁰Th/²³²Th ratio and thus was impractical in this study. The ²⁰⁷Pb/²³⁵U system is unaffected by excess radiogenic Pb; however, in young samples, low ²⁰⁷Pb abundance precludes precise age determination. Monazite ages presented on the map in Figure 6 use the ²⁰⁴Pb-corrected ²⁰⁸Pb/²³²Th system, which

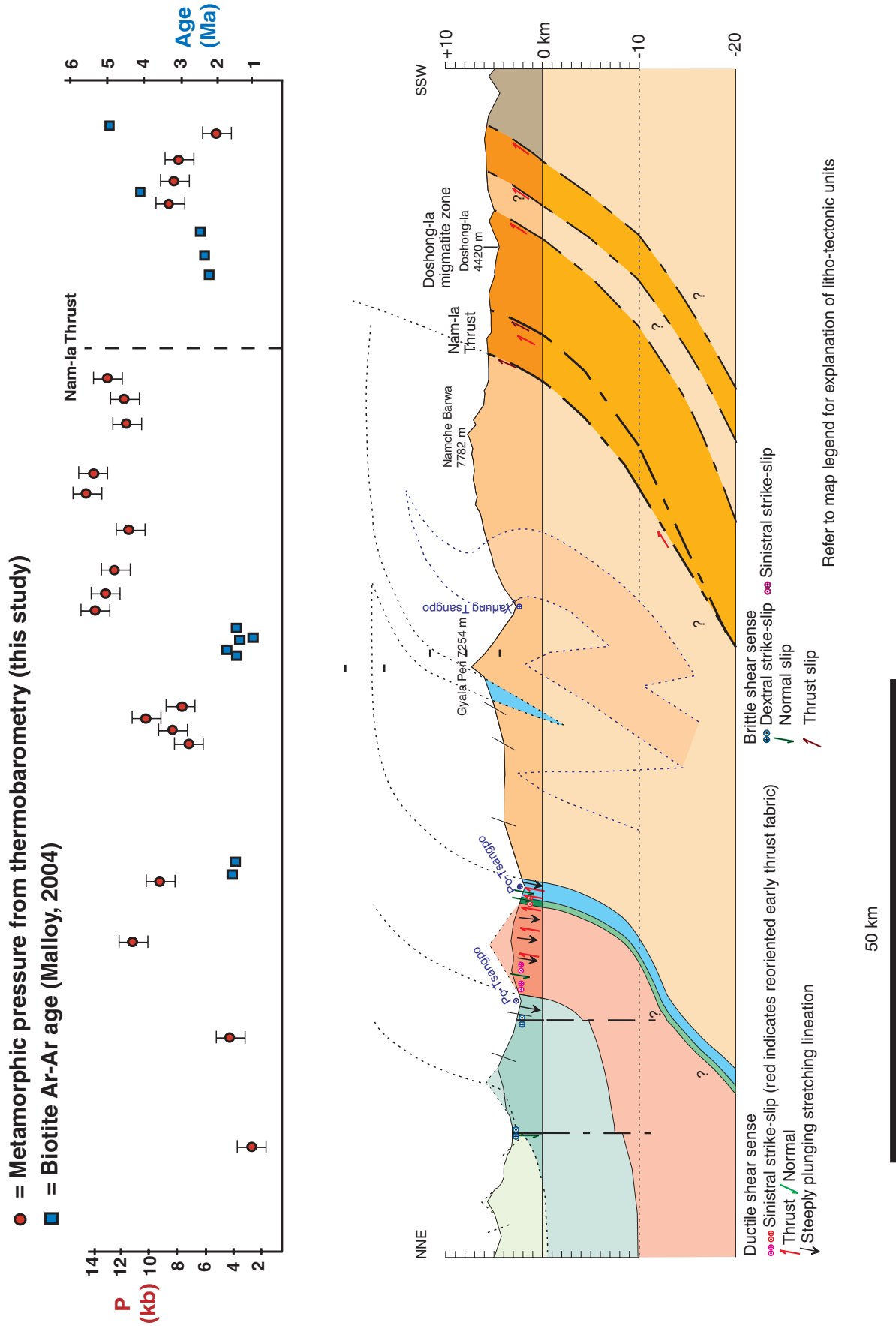


Figure 5. Structural cross section through Gyala Peri and Namche Barwa along the axis of the Namche Barwa antiform, illustrating the distribution of metamorphic pressures, cooling ages, and breaks in these patterns. Ar-Ar biotite ages are from Malloy (2004).

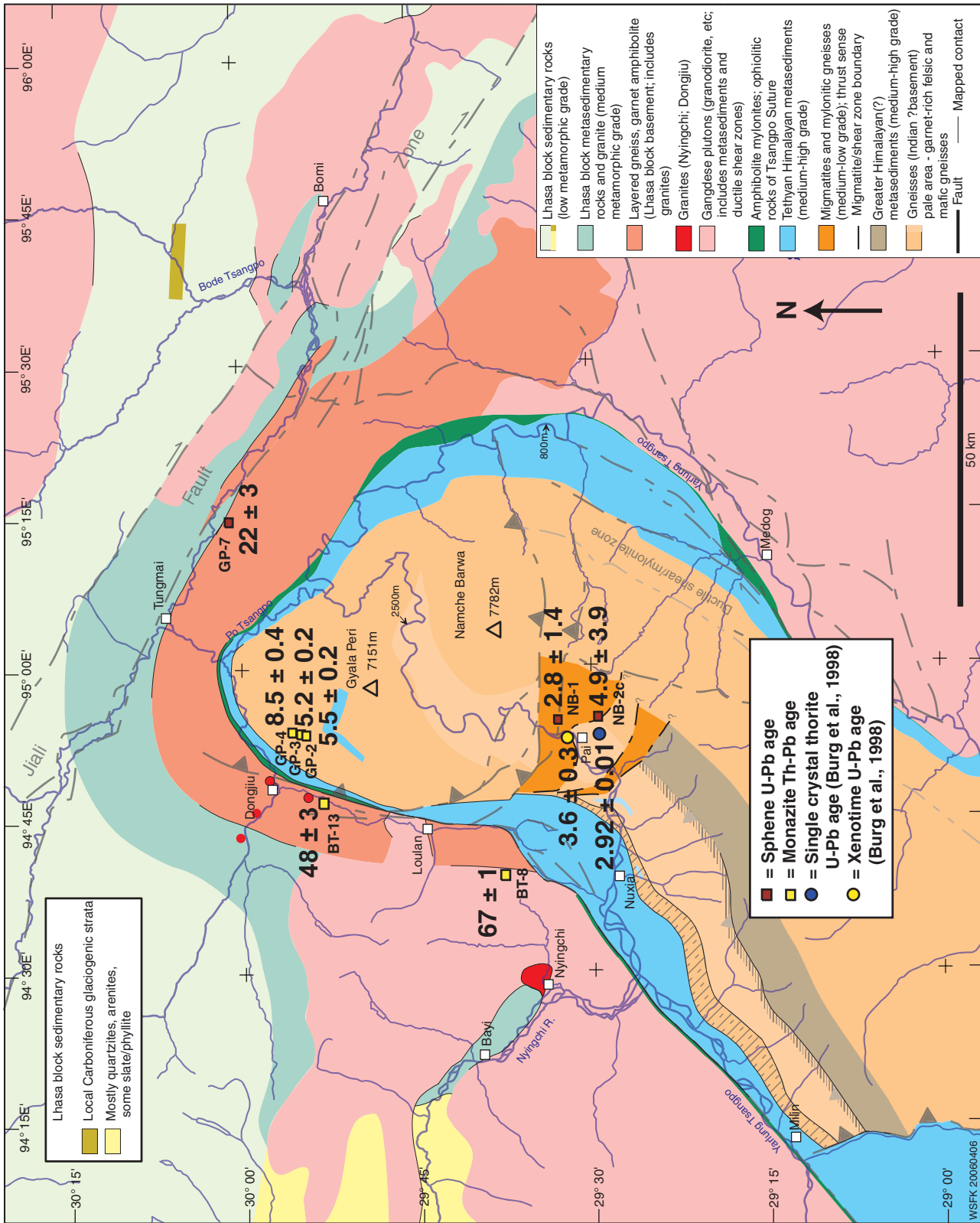


Figure 6. Th-Pb monazite ages shown on the Namche Barwa geologic map. Ages represent the weighted mean of the coherent age group determined by the data-reduction program, Squid, as detailed in the text.

allows for high count rates in parent and daughter isotopes, yielding precise ratio measurements. A potential isobaric interference at $m/e = 204$ (ThNdO_2^+) was identified by Ireland et al. (1999), which introduces uncertainty in the ^{204}Pb corrected isotopic ratio. We did not apply a correction for this interference, but agreement between uncorrected and corrected $^{208}\text{Pb}/^{232}\text{Th}$ ages suggests that this effect is less than the uncertainty of the measurement.

Weighted average Th-Pb monazite ages are presented on Tera-Wasserburg concordia diagrams in Figure 7, along with the 2σ age uncertainty, number of analyses constituting a coherent age group, and mean square of weighted deviates (MSWD) for the coherent group. Values of MSWD much greater than unity indicate uncertainty contributions that exceed analytical uncertainty and suggest that geologic variability such as outliers or samples from more than one population are contributing to the overall age range. Coherent age groups were extracted with Squid (Ludwig, 2001) using a minimum 5% probability-of-fit, and a minimum 30% fraction of the total analyses to constitute a valid age group. Analyses comprising the coherent age group are indicated on Figure 7. We confirmed these age groupings by plotting uncorrected U-Pb data on a Tera-Wasserburg diagram; coherent age groups generally lie on a linear array. However, discrepancies between U-Pb and the more robust Th-Pb ages may exist, due to the effect of ^{230}Th -derived excess ^{206}Pb (described above). Samples GP-2-04, GP-3-04, and GP-4-04 from the Gyala Peri region north of Namche Barwa yielded ages of 5.5 ± 0.2 Ma, 5.2 ± 0.2 Ma, and 8.5 ± 0.4 Ma, respectively. These ages are consistent with a ca. 8 Ma $^{40}\text{Ar}/^{39}\text{Ar}$ hornblende age reported by Ding et al. (2001). Two samples located outside the syntaxis (BT-8-01 and BT-13-01) had distinctly older ages of 67.0 ± 1.4 Ma and 47.5 ± 2.8 Ma, respectively.

Titanite Ages

Titanite is commonly used in U-Pb dating and has similar properties to monazite and zircon, with estimates of closure temperature ranging from 600 °C (Mezger et al., 1991) to 700 °C (Scott and St-Onge, 1995). Titanite was first applied as a dating tool by Tilton and Grunefelder (1968) and has since been widely applied to studies of polymetamorphic belts (e.g., Tucker et al., 1987). Titanite has been shown to retain Pb at temperatures in excess of crustal anatexis (Corfu, 1996; Zhang and Schärer, 1996), indicating that titanite ages from metamorphic terranes may reflect timing of late crystallization rather than cooling through the closure temperature (Bingen and van Breemen, 1998). Our U-Pb titanite ages are presented in

Table 2; all are ^{207}Pb -corrected $^{206}\text{Pb}/^{238}\text{U}$ values. Analysis of the youngest samples (NB-1-04, NB-2-04C, and GP-7-04) was hampered by a high concentration of common lead (Table 2), as is often the case with young metamorphic titanites. As such, the large errors of the U-Pb ages are mainly due to uncertainties in the common lead correction. However, when these samples are plotted on a conventional Wetherill concordia diagram (Fig. 8), the analyses spread out widely on a mixing-line trend toward the assumed common lead isotopic value. From the lower intercept of this line with the concordia, we were able to determine what we believe to be the “true” ages for NB-1-04, NB-2-04C, and GP-7-04 at 4.9 ± 3.9 Ma, 2.8 ± 1.4 Ma, and 21.7 ± 2.9 Ma, respectively. All monazite and titanite ages from this study are displayed on the map in Figure 6, together with thorite and xenotime age previously published by Burg et al. (1998).

Age Interpretation

Recent studies have shown that the interpretation of monazite ages requires knowledge of the chemical changes in monazite during metamorphism (e.g., Pyle et al., 2001; Spear and Pyle, 2002; Kohn and Malloy, 2004; Kohn et al., 2005). Th and Y act as particularly good tracers because their variation can be linked to silicate reactions (Kohn et al., 2005). BSE imaging and X-ray mapping of monazite grains prior to ion probe analysis allowed us to characterize the chemically distinguishable domains within each population (Figs. 11 and 12). Sample BT-8 is characteristic of rocks located outside the Namche Barwa massif, and shows bright areas under BSE corresponding to younger age populations. These bright regions are also enriched in Y and Th, as revealed by X-ray mapping (Figs. 11A and 11B). Yttrium content in monazite depends almost exclusively on reactions involving garnet (Pyle and Spear, 1999, 2003; Pyle et al., 2001), and so this zoning can be interpreted in terms of garnet growth history. In a study by Kohn et al. (2005), rim enrichment of Y is interpreted as newly grown monazite, formed as result of partial melting of a garnet-bearing host rock. Because monazite strongly partitions Y more than any other phase, and garnet liberates Y via dissolution during melt crystallization, new monazite growth tends to be higher in Y (Kohn et al., 2005). Inasmuch as partial melts have been documented throughout the entire Namche Barwa area (Burg et al., 1998; Ding et al., 2001; Booth et al., 2004), this interpretation makes sense in context of the regional metamorphic history. Thorium enrichment may be explained in a similar fashion—Th occurs in trace amounts in all common pelitic minerals, so would likely be liberated during dissolution of these phases and

partitioned into newly grown monazite. Sample GP-2, in contrast, is characteristic of Namche Barwa–Gyala Peri massif monazite, exhibiting virtually no variation in Y or Th (Figs. 11C and 11D). We interpret this to mean that these monazites formed during a single (recent) phase of metamorphism accompanied by garnet growth. This is supported by the narrow range of ages observed, both from mineral separates and from in-situ analysis of monazite in garnet.

Rocks from Namche Barwa have experienced a complex history of metamorphism. This, combined with the complexities of monazite geochronology, make interpretation of our U-Th-Pb monazite and titanite ages difficult. Several lines of evidence, however, suggest that these ages correspond to timing of prograde metamorphism: (1) Monazites and titanites are typically associated with metamorphic minerals, i.e., as inclusions in garnet or aluminosilicate. The presence of monazite does not appear to depend on metamorphic grade, and is more likely a function of bulk composition of the host rock than association with a particular metamorphic isograd. (2) In-situ ion microprobe analyses of monazite included in garnet (Fig. 9) yield ages similar to those obtained from analysis of separates, spanning a period of several million years (6.4 ± 0.3 Ma to 11.3 ± 0.2 Ma; Table 2). (3) The U-Th-Pb system in monazite is very resistant to diffusional exchange, and tends to remain unaffected at temperatures up to 900 °C (Cherniak et al., 2004). Therefore, metamorphic overprinting associated with rapid exhumation at lower temperatures should not have affected U-Th-Pb ages, unless the grains underwent fluid-mediated recrystallization. However, trace-element modeling of granites from within the Namche Barwa massif indicate melting under a dominantly fluid-absent regime (Booth et al., 2004). (4) Monazite and titanite ages correlate well with published granite ages, which are interpreted as crustal melts produced in concert with high-grade metamorphism and decompression-related anatexis (Burg et al., 1998; Ding et al., 2001; Booth et al., 2004). (5) The youngest monazite ages (from Gyala Peri) are homogeneous under BSE imaging (Figs. 10A and 10B), suggesting a single growth event, with no evidence for secondary recrystallization. Older ages, located outside the Namche Barwa massif, were obtained from grains that exhibit complex zoning under BSE imaging (Figs. 10C and 10D), indicating several growth and resorption episodes. This zoning was also observed in X-ray element maps of monazite (Fig. 11) as discussed above. For these zoned grains, we focused our analyses on bright regions in BSE images, typically found at the

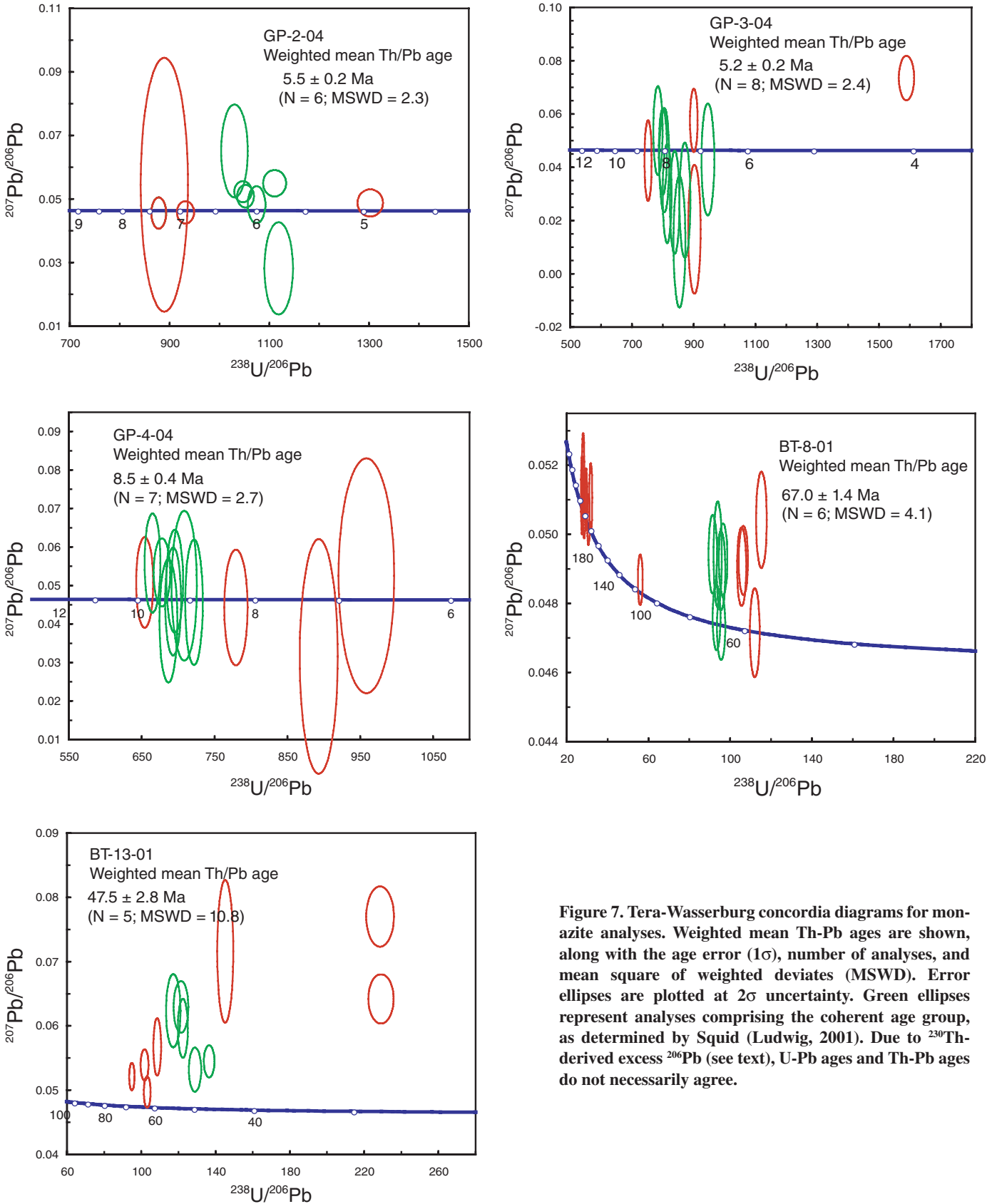


Figure 7. Tera-Wasserburg concordia diagrams for monazite analyses. Weighted mean Th-Pb ages are shown, along with the age error (1σ), number of analyses, and mean square of weighted deviates (MSWD). Error ellipses are plotted at 2σ uncertainty. Green ellipses represent analyses comprising the coherent age group, as determined by Squid (Ludwig, 2001). Due to ^{230}Th -derived excess ^{206}Pb (see text), U-Pb ages and Th-Pb ages do not necessarily agree.

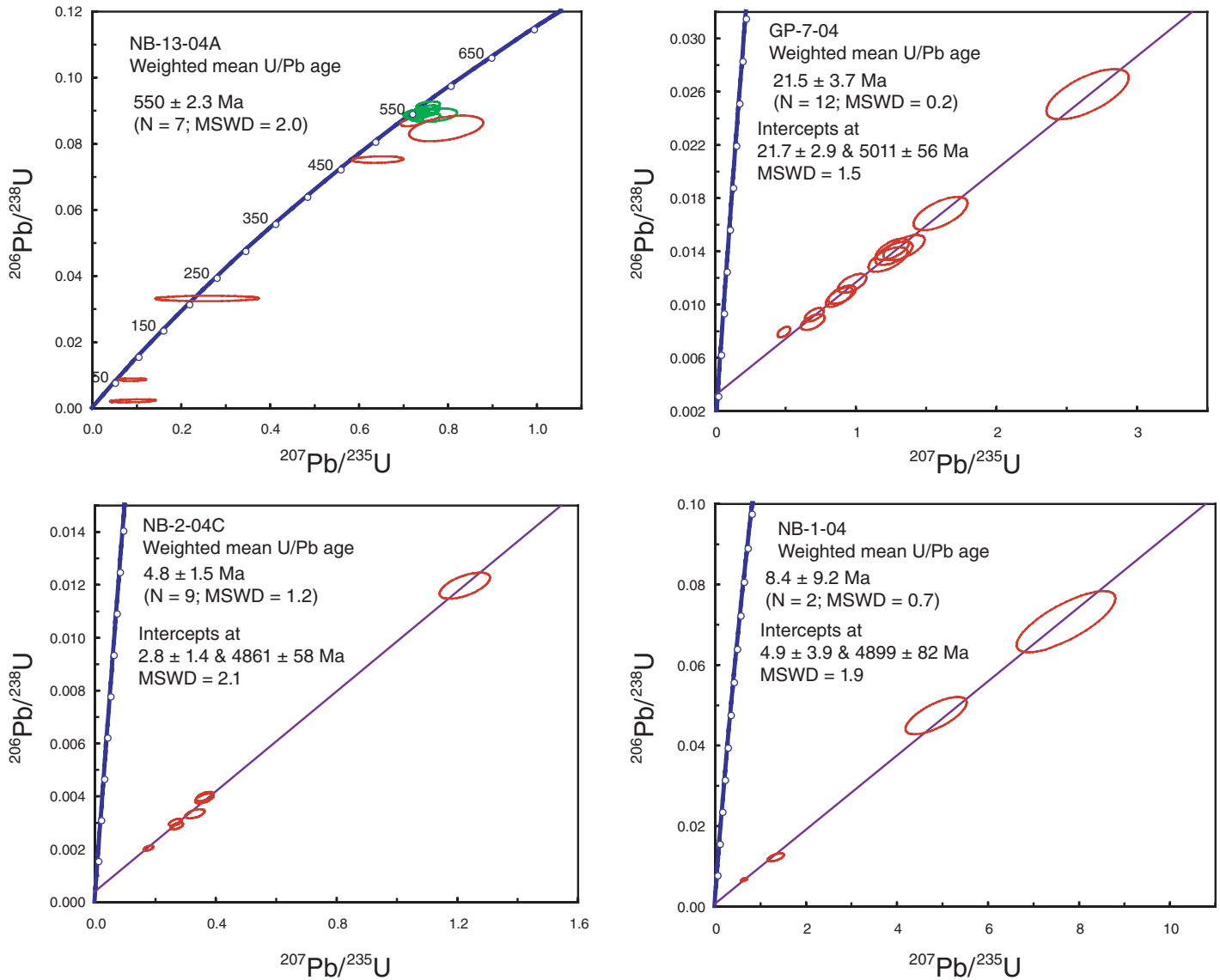


Figure 8. Wetherill concordia diagrams for titanite analyses. Weighted mean U-Pb ages are shown, along with the age error (\pm), number of analyses, and mean square of weighted deviates (MSWD). Error ellipses are plotted at 2σ uncertainty. For sample NB-13-04A, green ellipses represent analyses comprising the coherent age group, as determined by Squid (Ludwig, 2001). Intercepts of the common lead mixingline are shown for samples GP-7-04, NB-2-04C, and NB-1-04. The lower intercept of the mixing line represents the reported age for these threesamples.

rims of monazite and producing the youngest age population. Although many grains are fragmented as a result of mineral separation, internal zoning as revealed by BSE imaging and X-ray mapping allowed us to pinpoint generations of monazite in order to obtain a coherent age group. Thus, where composite populations seemed evident, the reported age (Fig. 6) represents the youngest generation of monazite.

Based on these arguments, we interpret the monazite and titanite ages to represent timing of prograde metamorphism within the various metamorphic terranes of the study area.

Inasmuch as monazite growth is known to occur over a broad range of conditions, spanning moderate to high-grade metamorphic rocks (Harrison et al., 2002), we believe this is a reasonable assumption. The range of ages observed from the eastern Himalayan syntaxis is probably a reflection of the multiple episodes of deformation affecting this area. An understanding of these ages can be achieved through our current knowledge of the tectono-metamorphic history of this region (i.e., Zhang et al., 1992; Burg et al., 1998; Ding et al., 2001; Booth et al., 2004).

Namche Barwa Metamorphic Ages

Monazite and titanite ages within the Namche Barwa massif are distinct from those exposed across the Indus Tsangpo suture zone. All ages inside Namche Barwa are less than 10 Ma, whereas rocks outside the massif have metamorphic ages exceeding 20 Ma. The young ages are distinct in the context of Himalayan metamorphism, which is primarily associated with Eocene initiation of collision of India with Asia. Only in select regions of the Himalaya are extremely young metamorphic ages documented, such as the central Himalaya, where

Th-Pb monazite ages of 3–10 Ma are reported associated with slip along the Main Central thrust (Harrison et al., 1997; Kohn et al., 2001; Catlos et al., 2001, 2002). These ages, however, correspond to P-T conditions (7 kbar and 550 °C) that are distinctly lower than those observed within Namche Barwa. In the western Himalayan syntaxis, monazite ages of 4–11 Ma have been reported from Nanga Parbat (Smith et al., 1992) in association with amphibolite- to granulite-grade metamorphism. This recent metamorphism at Nanga Parbat coincides with leucogranite production (Zeitler and Chamberlain, 1991) as well as the onset of rapid denudation (Zeitler, 1985; Zeitler et al., 1989), suggesting a causal relationship involving positive feedbacks between surficial and tectonic processes (e.g., Zeitler et al., 2001b). Our monazite and titanite ages also correspond with timing of granitic melt emplacement at Namche Barwa (Burg et al., 1998; Ding et al., 2001; Booth et al., 2004; Fig. 12), and support the evidence for a high-grade metamorphism and melting event during this time. Metamorphic ages are therefore likely associated with the same processes that produced these melts, i.e., rapid denudation and anatexis.

There is an interesting variation within the Namche Barwa ages (Fig. 6), where younger ages (3–5 Ma) are observed in the southern part of the massif and slightly older ages (6–10 Ma) are located north, near Gyala Peri. We interpret this as a reflection of the dated mineral (i.e., monazite versus titanite, thorite, or xenotime) and their differences in closure temperature, rather than a distinct difference in age of metamorphism. Thus, all metamorphic ages from Namche Barwa–Gyala Peri are interpreted as dating the same (young) event.

We cannot rule out the possibility that an early Himalayan metamorphic episode affected these rocks and was later overprinted by the recent, high-grade metamorphic event. If so, the highest grade rocks might be analogous to the Kaghan and Tso Moriri crustal slices in the western Himalaya—subducted deeply and then returned back through the crustal subduction zone. Therefore, any ages and/or high-pressure (HP) assemblages recording such an event are not seen, as they were subsequently erased by the most recent phase of metamorphism.

Ages outside Namche Barwa

Across the suture zone, all metamorphic ages are distinctly Himalayan in origin. The two oldest ages (48 ± 3 Ma and 67 ± 1 Ma) are associated with Gangdese plutonism resulting from subduction of Tethyan lithosphere beneath Asia. Diorites and granodiorites from the eastern section of the Gangdese batho-

lith yield isotopic ages between 113 ± 2 Ma ($^{40}\text{Ar}/^{39}\text{Ar}$ method on amphiboles; Maluski et al., 1988) and 41.1 ± 0.4 Ma (U/Pb method on zircons; Schärer et al., 1984). Near the Namche Barwa syntaxis, within the Lhasa block of this region, numerous granitoids have U-Pb zircon ages of 40–70 Ma and ca. 120 Ma (Booth et al.,

2004), which are also attributed to Gangdese arc plutonism.

The 22 ± 3 Ma titanite age could have several interpretations, inasmuch as multiple events ca. 18–25 Ma are known to have affected the eastern Himalayan syntaxis. Magmatism has been documented along the Red River shear

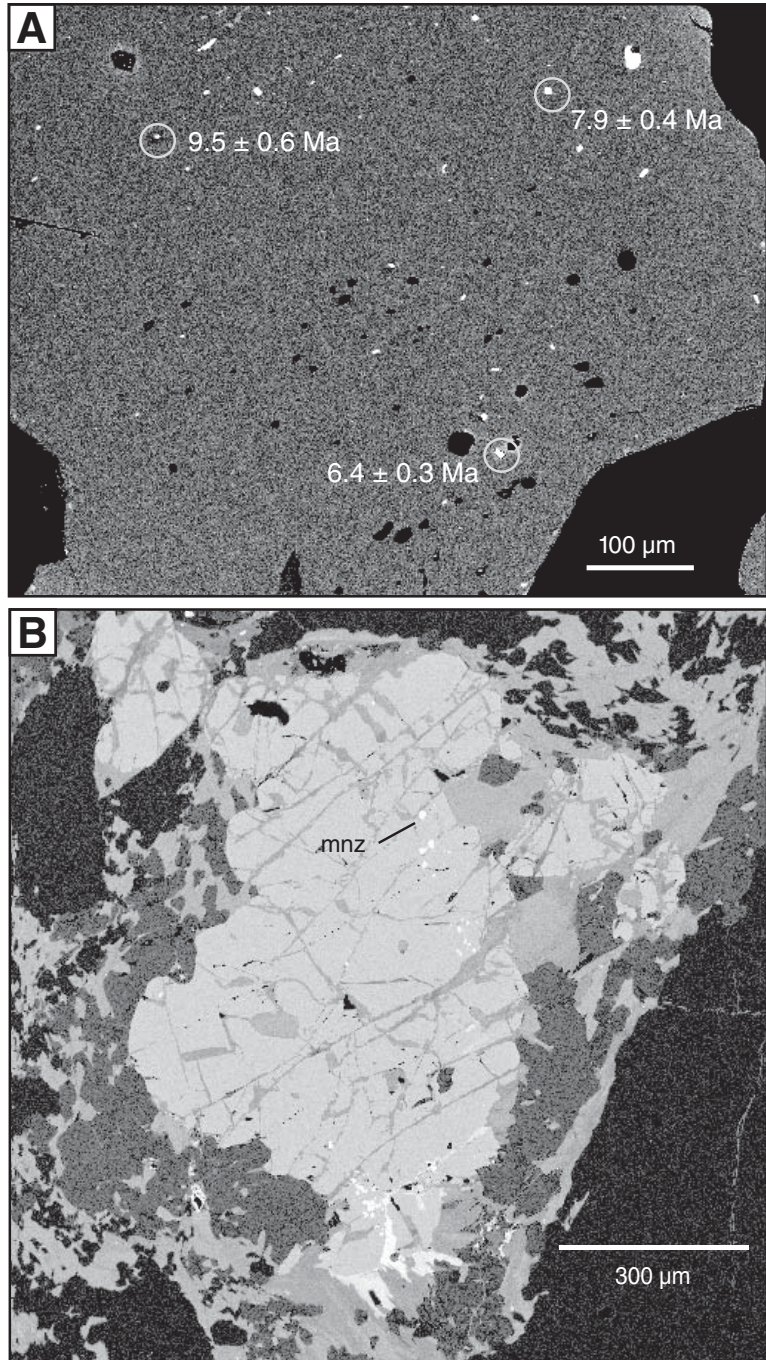


Figure 9. Backscattered-electron (BSE) images of monazite inclusions in garnet from sample GP-4-04: (A) showing actual grains dated and Th-Pb ages and (B) in thin section.

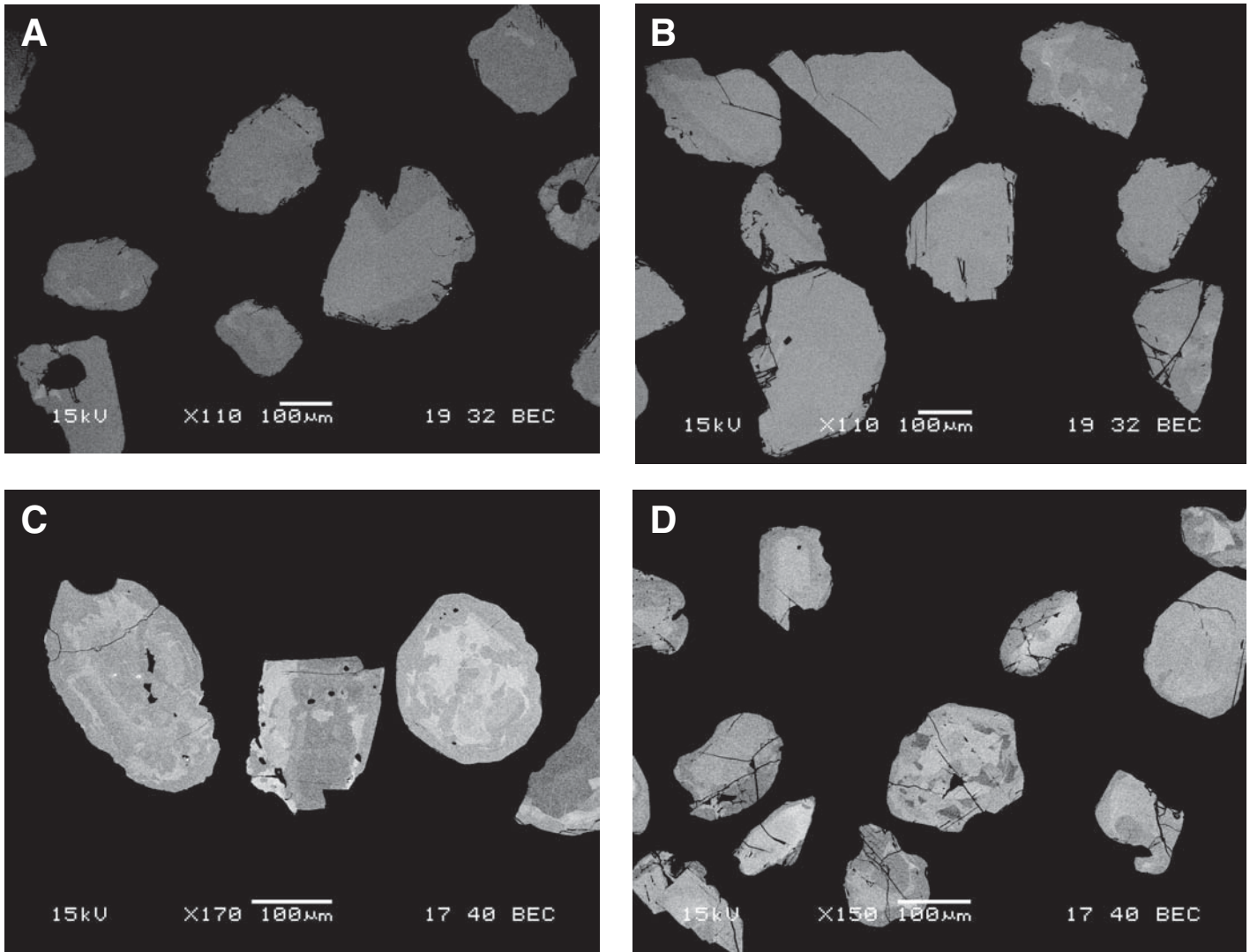


Figure 10. Backscattered-electron (BSE) images of monazite separates: (A) GP-3, (B) GP-4, (C) BT-8, (D) BT-13.

zone (e.g., Zhang and Schärer, 1999; Leloup and Kienast, 1993), with partial melt emplacement ages ca. 22–23 Ma. It is possible that the 22 ± 3 Ma age is associated with shear-induced metamorphism as part of this event. However, it could also be related to the Gangdese thrust event, which is of this age (ca. 27–18 Ma) and involved underthrusting of part of the Gangdese belt (Copeland et al., 1995; Yin et al., 1994; Yin et al., 1999; Harrison et al., 2000).

DISCUSSION

Our P-T estimates and metamorphic ages show several interesting characteristics. The most prominent is that across the Indus Tsangpo suture zone there is a distinct break in metamorphic assemblages, peak P-T estimates,

and metamorphic ages. Within Namche Barwa, thermobarometry on garnet-biotite-plagioclase assemblages indicates peak metamorphic pressures and temperatures of 10–15 kbar and 700–900 °C in the core of the massif. These high-grade assemblages correspond to the youngest (<10 Ma) metamorphic ages. Monazite and titanite from Namche Barwa gneisses give Th-Pb and U-Pb ages of 3–10 Ma. Outside of Namche Barwa, however, P-T estimates are lower (4–10 kbar and <800 °C), and all ages are distinctly older. Th-Pb monazite ages of Lhasa Block metasediments are between 40 and 70 Ma, corresponding to Gangdese plutonism. However, the younger (22 ± 3 Ma) titanite age in this area must be associated with a more recent metamorphic event, possibly related to slip along the Gangdese thrust.

Within the Namche Barwa massif, metamorphic ages are consistently less than 10 Ma, and thus are distinct from periods of metamorphism reported elsewhere in the Himalayas, with exceptions noted above. The young monazites and titanites correspond with ages of granitic melts in this area (Burg et al., 1998; Ding et al., 2001; Booth et al., 2004), which have a distinctive geochemical signature. Whole-rock geochemistry (e.g., Booth et al., 2004) based on Rb/Sr ratios indicates that these granitoids are products of decompression melting. It has been shown (Harris et al., 1993; Whittington et al., 1999) that trace-element abundances in granitic rocks can provide information regarding the conditions prevalent during melting. Geochemical modeling of Rb and Sr during anatexis suggests that fluid-absent breakdown of muscovite

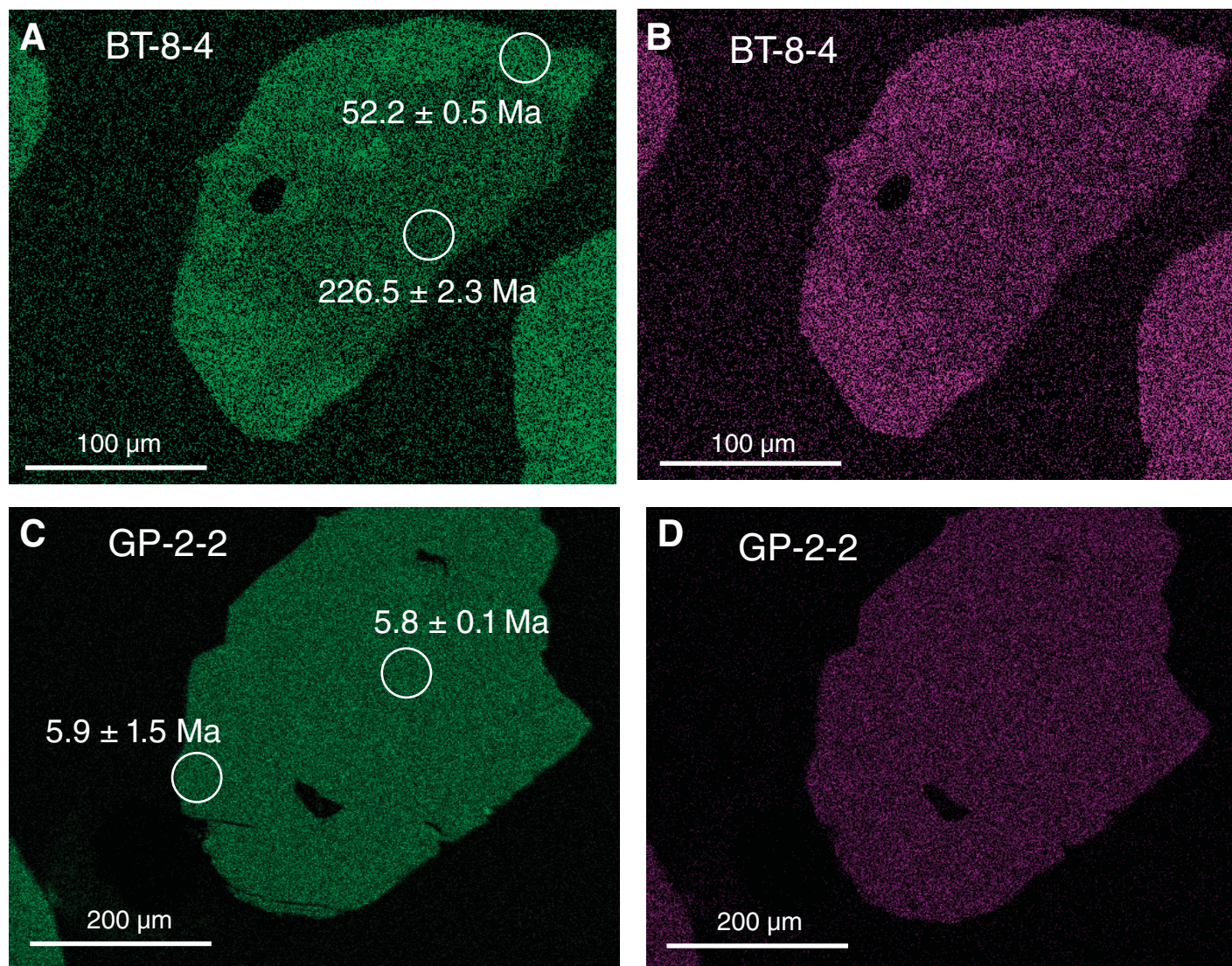


Figure 11. X-ray element maps of representative monazite samples, BT-8: (A) Y content and (B) Th content; and GP-2: (C) Y content and (D) Th content.

would produce melts with Rb/Sr ratios >1.5 (Harris and Inger, 1992). Granitoids from within Namche Barwa exhibit relatively high Rb/Sr ratios (>1.4) suggesting that a fluid-absent melting (decompression) regime dominates near the massif core. Meanwhile, granitoids from outside Namche Barwa exhibit Rb/Sr ratios consistently below 1.5 and imply fluid-present melting in the surrounding regions (Booth et al., 2004).

The other salient feature of our data is that a systematic variation in both P-T and metamorphic ages exists within Namche Barwa itself (Fig. 6). The data suggest a metamorphic break across the Nam-la thrust, separating high-grade rocks to the north from lower grade rocks to the south. Rocks north of the Nam-la thrust equilibrated at pressures of 11–14 kbar, which requires that up to 40 km of crust be removed

since 3–10 Ma. Namche Barwa gneisses cover an area of ~ 2000 km². Assuming a crustal density of 2.8 g/cm³, this implies up to 2×10^{14} kg of crust have been removed in the past 3–10 Myr. Moreover, in-situ monazite ages combined with thermobarometry on rocks from Gyala Peri indicate garnet growth occurred over several million years (6.4 ± 0.3 Ma to 11.3 ± 0.2 Ma; sample GP-4, Table 2) and during a pressure decrease of ~ 5 kbar (GP-4 core = 8.3 kbar; rim = 3.5 kbar, Table 1). These pressure-temperature changes are summarized in Figure 13, and suggest long-term exhumation rates of at least ~ 3 mm/yr. A mechanism for transporting such a large amount of material to the surface remains unclear. We take this opportunity to examine our results in the context of different geodynamical models, which link surface processes to patterns of

crustal deformation and exposure of metamorphic facies.

The Himalayan syntaxis have been attributed to oroclinal bending (Ratschbacher et al., 1994), lithospheric-scale folding (e.g., Treloar et al., 1991; Burg et al., 1998; Burg and Podladchikov, 1999), duplex thrusting (e.g., Ding et al., 2001; Yin et al., 2006) and/or a pop-up structure (Schneider et al., 1999; Poage et al., 2000). However, not all of these models are focused on the eastern Himalayan syntaxis in particular, and we emphasize that the structural development of Nanga Parbat and Namche Barwa are not necessarily analogous. Of these studies, Burg et al. (1998) is most consistent with our observations that the eastern Himalayan syntaxis is folded into a lithospheric-scale antiform, the structural evolution of which controlled the earlier portion

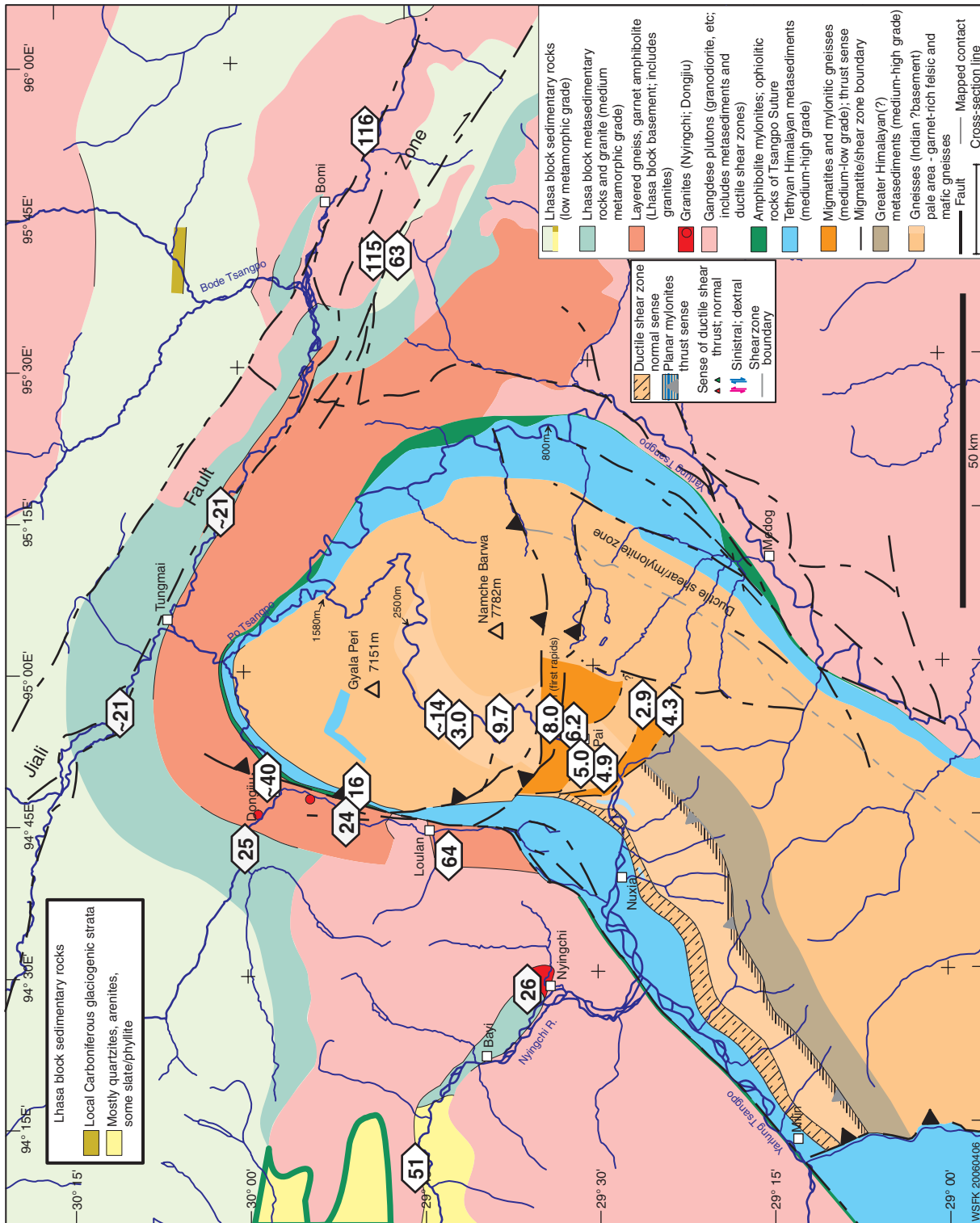


Figure 12. Compiled map of U-Pb granite ages from the Namche Barwa area (after Booth et al., 2004).

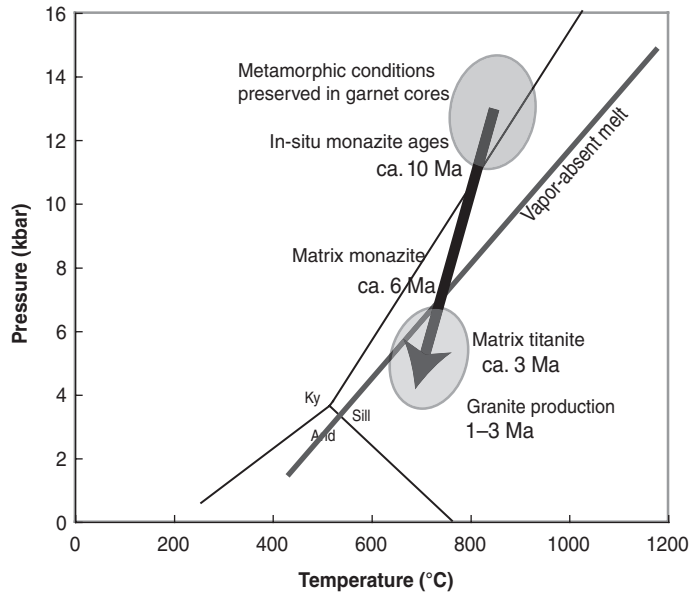


Figure 13. Generalized pressure-temperature-time (P-T-t) diagram, showing growth of garnet, monazite, and titanite and the timing of melting within the Namche Barwa region.

of Namche Barwa's history. All of these models, however, assign a passive role to major rivers that crosscut the orogen. In contrast, many recent studies suggest that the Tsangpo was not antecedent to the Namche Barwa structure but rather drove exhumation of the massif as part of a late Miocene capture event (Koons, 1995; Brookfield, 1998; Clark et al., 2004). Models coupling erosional and tectonic processes (e.g., Jamieson and Beaumont, 1989; Beaumont et al., 1992; Koons, 1995; Koons et al., 2002) are therefore more appropriate to consider as viable models for interpretation of our data set.

This study reports high-grade metamorphism roughly coincident with the age of decompression melting (Booth et al., 2004; Fig. 12), as well as a period of rapid denudation at Namche Barwa, estimated at up to ~10 mm/yr over the past 3 Myr (Burg et al., 1998). Coincidence of young granite intrusion with a period of rapid erosion suggests a cause-effect relationship, perhaps a scenario involving decompression melting that mimics Nanga Parbat in the western Himalayan syntaxis. Younger cooling ages also correspond to high-P metamorphism (Fig. 5), indicating rapid exhumation accompanied by high-grade metamorphism. Young activity and decompression melts are features characteristic of a "tectonic aneurysm" model (Zeitler et al., 2001a; Koons et al., 2002), which attributes anatexis and high-grade metamorphism to rapid exhumation initiated by the Yarlung Tsangpo.

Coupled thermal-mechanical-erosional modeling (Koons et al., 1998; Zeitler et al., 2001b; Koons et al., 2002) shows that in a deforming orogen, local rheological variations will arise from deep and rapid incision. The crust will weaken as the strong upper crust is locally stripped from above by erosion, and the local geotherm is then steepened from below by a responding focused rapid uplift of hot rock. Provided that efficient erosion continues, a positive feedback develops in which flow of material into this weakened zone maintains local elevation and relief, reinforcing the concentrated exhumation and bowing up isotherms. This feedback model has been dubbed a "tectonic aneurysm" (Zeitler et al., 2001a), in the sense of self-sustained failure of a normally strong boundary. Inherent in this model is the notion that feedback can amplify rather local geomorphic processes to the point where they exert a profound influence on the metamorphic and structural evolution of rocks at considerable depth. The tectonic aneurysm proposes that even at local scales of ~20 km, strong feedbacks can develop between fluvial erosion and crustal deformation, such that strain is increasingly localized, resulting in formation and exposure of a high-grade metamorphic massif. Young metamorphic ages and high P-T equilibrium conditions near the core of Namche Barwa seem to support this model. Our data also suggest that these tectonic-surficial feedbacks have been operative since at least 3 Ma (and perhaps since ca. 10 Ma), implying that Namche Barwa is not merely a recent,

transient feature in the crust. This is supported by drainage patterns of rivers in eastern Tibet, which indicate that river capture and reversal occurred prior to or coeval with Miocene uplift of this area (Brookfield, 1998; Hallet and Molnar, 2001; Clark et al., 2004).

The tectonic aneurysm model is a specifically localized interpretation of the tectono-metamorphic features of our data set. A related but alternative possibility is that rapid exhumation observed at Namche Barwa is accomplished through widespread ductile extrusion, in the context of channel flow from beneath Tibet. Models of the Himalayan-Tibetan system (e.g., Royden et al., 1997; Clark and Royden, 2000) portray the Tibetan Plateau as underlain by a weak lower crust, decoupled from upper crustal deformation, and outward growth of the Tibetan Plateau has been proposed to occur through eastward extrusion of the lower crust (Royden, 1996; Clark and Royden, 2000; Shen et al., 2001). Coupled erosional-tectonic modeling (e.g., Beaumont et al., 1992; Beaumont et al., 2001) suggests that focused erosion at the edge of a plateau underlain by low-viscosity material can lead to ductile extrusion of high-grade metamorphic rocks between bounding structures. This coupling is proposed to be responsible for exhumation of the Greater Himalayan Sequence during the Miocene, between the Main Central thrust and South Tibetan detachment system (Beaumont et al., 2001). The location of Namche Barwa at the southeastern edge of the Tibetan Plateau, combined with erosion rates that are among the highest in the world (Singh and France-Lanord, 2002), suggests that similar processes may have influenced the evolution of the eastern Himalayan syntaxis. It is possible that the high-grade metamorphic rocks of Namche Barwa were brought to the surface through ductile extrusion facilitated by a low-viscosity crustal channel from beneath Tibet. If so, the Nam-la thrust system, and possibly other unidentified similar structures, must be involved in accommodating this motion. Ductile extrusion might therefore be a process that has been active here since the late Miocene. However, the channel-flow model implies that the material being extruded is derived, at least in part, from beneath Tibet. If this were the case, one would expect to see evidence at Namche Barwa of Asian plate rocks, i.e., Lhasa Block material and/or a Gangdese arc signature within the Indian basement gneisses; to our knowledge, this has not yet been observed in this region.

Our data are consistent with the lithospheric-scale buckling model of Burg et al. (1998). However, currently existing geodynamic models have the ability to integrate many geological and geophysical observations, linking lithospheric

deformation with surface denudation to predict how crustal rheology might be affected by river erosion. It is beyond the scope of this paper to prove or disprove these models. Nevertheless, our data appear to most closely fit the tectonic aneurysm model (Zeitler et al., 2001a; Koons et al., 2002), based on distinct spatial correlations between P-T conditions, age of metamorphism, and erosion by the Tsangpo. Surficial-tectonic interactions on the order of ~20 km are consistent with the scales predicted by this model. The ductile extrusion model (Beaumont et al., 1992; Beaumont et al., 2001) also cannot be ruled out entirely with the existing data, particularly for earlier parts of the exhumation history.

ACKNOWLEDGMENTS

This research was funded by grants from the National Science Foundation, Earth Sciences Division, Continental Dynamics Program awarded to C.P. Chamberlain (EAR-0003530), P.K. Zeitler (EAR-0003462), and W.S.F. Kidd (EAR-0003673). This paper benefited greatly from comments by A. Mulch, W.G. Ernst, and M. McWilliams on an earlier version, as well as constructive critiques by two anonymous reviewers. We thank colleagues at the Chengdu Institute of Geology and Mineral Resources, particularly Tang Wenqing, Liu Yuping, and Zhang Xuanyang, for indispensable help with logistics and fieldwork. We also thank Joe Wooden and Frank Mazdab for help with monazite and titanite SHRIMP analysis.

REFERENCES CITED

- Aleinikoff, J.N., Schenck, W.S., Plank, M.O., Srogi, L., Fanning, C.M., Kamo, S.L., and Bosbyshell, H., 2006, Deciphering igneous and metamorphic events in high-grade rocks of the Wilmington Complex, Delaware: Morphology, cathodoluminescence and backscattered electron zoning, and SHRIMP U-Pb geochronology of zircon and monazite: *Geological Society of America Bulletin*, v. 118, p. 39–64, doi: 10.1130/B25659.1.
- Aleinikoff, J.N., Wintsch, R.P., Tollo, R.P., Unruh, D.M., Fanning, C.M., and Schmitz, M.D., 2007, Ages and origins of rocks of the Killingworth Dome, south-central Connecticut: Implications for the tectonic evolution of southern New England: *American Journal of Science*, v. 307, p. 63–118, doi: 10.2475/01.2007.04.
- Azor, A., Simancas, J.F., Exposito, I., Lodeiro, F.G., and Poyatos, D.J.M., 1997, Deformation of garnets in a low-grade shear zone: *Journal of Structural Geology*, v. 19, p. 1137–1148, doi: 10.1016/S0191-8141(97)00040-0.
- Bea, F., and Montero, P., 1999, Behavior of accessory phases and redistribution of Zr, REE, Y, Th, and U during metamorphism and partial melting of metapelites in the lower crust: An example from the Kinzigite Formation of Ivrea-Verbanò, NW Italy: *Geochimica et Cosmochimica Acta*, v. 63, p. 1133–1153, doi: 10.1016/S0016-7037(98)00292-0.
- Beaumont, C., Fullsack, P., and Hamilton, J., 1992, Erosional control of active compressional orogens, in McClay, K.R., ed., *Thrust tectonics*: London, Chapman and Hall, p. 1–18.
- Beaumont, C., Jamieson, R.A., Nguyen, M.H., and Lee, B., 2001, Himalayan tectonics explained by extrusion of a low-viscosity crustal channel coupled to focused surface denudation: *Nature*, v. 414, p. 738–742, doi: 10.1038/414738a.
- Beaumont, C., Jamieson, R.A., Nguyen, M.H., and Medvedev, S., 2004, Crustal channel flows: 1. Numerical models with applications to the tectonics of the Himalayan-Tibetan orogen: *Journal of Geophysical Research*, v. 109, p. B06406, doi: 10.1029/2003JB002809.
- Bingen, B., and van Breemen, O., 1998, U-Pb monazite ages in amphibolite- to granulite-facies orthogneiss reflect hydrous mineral breakdown reactions: Sveconorwegian Province of SW Norway: *Contributions to Mineralogy and Petrology*, v. 132, p. 336–353, doi: 10.1007/s004100050428.
- Bingen, B., Demaiffe, D., and Hertogen, J., 1996, Redistribution of rare earth elements, thorium, and uranium over accessory minerals in the course of amphibolite to granulite facies metamorphism: The role of apatite and monazite in orthogneisses from southwestern Norway: *Geochimica et Cosmochimica Acta*, v. 60, p. 1341–1354, doi: 10.1016/0016-7037(96)00006-3.
- Booth, A.L., Zeitler, P.K., Kidd, W.S.F., Wooden, J., Lui, Y., Idleman, B., Hren, M., and Chamberlain, C.P., 2004, U-Pb zircon constraints on the tectonic evolution of southeastern Tibet, Namche Barwa area: *American Journal of Science*, v. 304, p. 889–929, doi: 10.2475/ajs.304.10.889.
- Brookfield, M.E., 1998, The evolution of the great river systems of southern Asia during the Cenozoic India-Asia collision: Rivers draining southwards: *Geomorphology*, v. 22, p. 285–312, doi: 10.1016/S0169-555X(97)00082-2.
- Burchfiel, B.C., King, R., Royden, L.H., Wang, E., Chen, Z., Zhang, X., and Zhao, J., 1998, Tectonic interpretation of GPS results from the SE part of the Tibetan Plateau and within the European/Asian framework: *Geological Society of America Abstracts with Programs*, v. 30, p. 108.
- Burg, J.-P., and Podladchikov, Y., 1999, Lithospheric scale folding: Numerical modeling and application to the Himalayan syntaxis: *International Journal of Earth Sciences*, v. 88, p. 190–200, doi: 10.1007/s005310050259.
- Burg, J.P., Nievèrgelt, P., Oberli, F., Seward, D., Davy, P., Maurin, J.-C., Diao, Z., and Meier, M., 1998, The Namche-Barwa syntaxis: Evidence for exhumation related to compressional crustal folding: *Journal of Asian Earth Sciences*, v. 16, p. 239–252, doi: 10.1016/S0743-9547(98)00002-6.
- Catlos, E.J., Harrison, T.M., Kohn, M.J., Grove, M., Lovera, O.M., Ryerson, F.J., and Upreti, B.N., 2001, Geochronologic and thermobarometric constraints on the evolution of the Main Central thrust, central Nepal Himalaya: *Journal of Geophysical Research*, v. 106, p. 16,177–16,203, doi: 10.1029/2000JB900375.
- Catlos, E.J., Harrison, T.M., Manning, C.E., Grove, M., Rai, S.M., Hubbard, M.S., and Upreti, B.N., 2002, Records of the evolution of the Himalayan orogen from in-situ Th-Pb ion microprobe dating of monazite: Eastern Nepal and western Garhwal: *Journal of Asian Earth Sciences*, v. 20, p. 459–479, doi: 10.1016/S1367-9120(01)00039-6.
- Chen, Z., Liu, Y., Hodges, K.V., Burchfiel, B.C., Royden, L.H., and Deng, C., 1990, Structural evolution of the Kangmar dome: A metamorphic core complex in southern Xizang (Tibet): *Science*, v. 250, p. 1552–1556, doi: 10.1126/science.250.4987.1552.
- Cherniak, D.J., Watson, E.B., and Grove, M., 2004, Pb diffusion in monazite: A combined RBS/SIMS study: *Geochimica et Cosmochimica Acta*, v. 68, p. 829–840.
- Clark, M.K., and Royden, L.H., 2000, Topographic ooze: Building the eastern margin of Tibet by lower crustal flow: *Geology*, v. 28, p. 703–706, doi: 10.1130/0091-7613(2000)28<703:TOBTEM>2.0.CO;2.
- Clark, M.K., Schoenbohm, L.M., Royden, L.H., Whipple, K.X., Burchfiel, B.C., Zhang, X., Tang, W., Wang, E., and Chen, L., 2004, Surface uplift, tectonics, and erosion of eastern Tibet from large-scale drainage patterns: *Tectonics*, v. 23, p. TC1006, doi: 10.1029/2002TC001402.
- Copeland, P., Harrison, T.M., Yun, P., Kidd, W.S.F., Roden, M., and Zhang, Y., 1995, Thermal evolution of the Gangdese Batholith, southern Tibet: A history of episodic unroofing: *Tectonics*, v. 14, p. 223–236, doi: 10.1029/94TC01676.
- Corfu, F., 1996, Multistage zircon and titanite growth and inheritance in an Archean gneiss complex, Winnipeg River Subprovince, Ontario: *Earth and Planetary Science Letters*, v. 141, p. 175–186, doi: 10.1016/0012-821X(96)00064-7.
- DeWolf, C.P., Belshaw, N., and O’Nions, R.K., 1993, A metamorphic history from micron-scale ²⁰⁷Pb-²⁰⁶Pb chronometry of Archean monazite: *Earth and Planetary Science Letters*, v. 120, p. 207–220, doi: 10.1016/0012-821X(93)90240-A.
- Ding, L., Zhong, D., Yin, A., Kapp, P., and Harrison, T.M., 2001, Cenozoic structural and metamorphic evolution of the eastern Himalayan syntaxis (Namche Barwa): *Earth and Planetary Science Letters*, v. 192, p. 423–438, doi: 10.1016/S0012-821X(01)00463-0.
- Ferry, J.M., 2000, Patterns of mineral occurrence in metamorphic rocks: *American Mineralogist*, v. 85, p. 1573–1588.
- Foster, G., Kinny, P., Vance, D., Prince, C., and Harris, N., 2000, The significance of monazite U-Th-Pb age data in metamorphic assemblages: a combined study of monazite and garnet chronometry: *Earth and Planetary Science Letters*, v. 181, p. 327–340, doi: 10.1016/S0012-821X(00)00212-0.
- Geng, Q.R., Pan, G.T., Zheng, L.L., Chen, Z.L., Fisher, R.D., Sun, Z.M., Ou, C.S., Dong, H., Wang, X.W., Li, S., Lou, X.Y., and Fu, H., 2006, The eastern Himalayan syntaxis: Major ophiolitic mélanges and geologic evolution: *Journal of Asian Earth Sciences*, v. 27, p. 265–285, doi: 10.1016/j.jseas.2005.03.009.
- Guillot, S., Pochat, S., Zakarain, N., and Hodges, K.V., 1998, Metamorphic evolution of the Kangmar Dome (Se-Xizang, Southern Tibet): Implications for the internal Himalayan zones: *Comptes Rendus des Academies des Sciences—Sciences de la Terre et des Planetes*, v. 327, p. 577–582.
- Hallet, B., and Molnar, P., 2001, Distorted drainage basins as markers of crustal strain east of the Himalaya: *Journal of Geophysical Research*, v. 106, p. 13,697–13,709, doi: 10.1029/2000JB900335.
- Harris, N.B.W., and Inger, S., 1992, Trace element modeling of pelite-derived granites: *Contributions to Mineralogy and Petrology*, v. 110, p. 46–56, doi: 10.1007/BF00310881.
- Harris, N.B.W., Inger, S., and Massey, J., 1993, The role of fluids in the formation of High Himalayan leucogranites, in Treloar, P.J., and Searle, M.P., *Himalayan tectonics: The Geological Society of London Special Publication*, v. 74, p. 391–400.
- Harrison, T.M., Ryerson, F.J., Le Fort, P., Yin, A., Lovera, O.M., and Catlos, E.J., 1997, A late Miocene-Pliocene origin for central Himalayan inverted metamorphism: *Earth and Planetary Science Letters*, v. 146, p. E1–E8, doi: 10.1016/S0012-821X(96)00215-4.
- Harrison, T.M., Yin, A., Grove, M., Lovera, O.M., Ryerson, F.J., and Xinhua, Z., 2000, The Zedong Window: A record of superposed Tertiary convergence in south-eastern Tibet: *Journal of Geophysical Research*, v. 105, p. 19,211–19,230, doi: 10.1029/2000JB900078.
- Harrison, T.M., Catlos, E.J., and Montel, J.-M., 2002, U-Th-Pb dating of phosphate minerals, in Kohn, M.J., Rakovan, J., and Hughes, J.M., eds., *Phosphates: Geochemical, geological and materials importance: Reviews in Mineralogy and Geochemistry*, v. 48, p. 523–558.
- Hodges, K.V., 2000, Tectonics of the Himalaya and southern Tibet from two perspectives: *Geological Society of America Bulletin*, v. 112, p. 324–350, doi: 10.1130/0016-7606(2000)112<0324:TOTHAS>2.3.CO;2.
- Holland, T.J.B., and Powell, R., 1998, An internally consistent thermodynamic data set for phases of petrological interest: *Journal of Metamorphic Geology*, v. 16, p. 309–343, doi: 10.1111/j.1525-1314.1998.00140.x.
- Ireland, T.R., and Williams, I.S., 2003, Considerations in zircon geochronology by SIMS, in Hanchar, J.M., and Hoskins, P.W.O., eds., *Zircon: Reviews in Mineralogy and Geochemistry*, v. 53, p. 215–241.
- Ireland, T.R., Wooden, J.L., Persing, H., and Ito, B., 1999, Geological applications and analytical development of the SHRIMP RG: *Eos (Transactions, American Geophysical Union)*, v. 80, p. 1117.
- Jamieson, R.A., and Beaumont, C., 1989, Deformation and metamorphism in convergent orogens: A model for uplift and exhumation of metamorphic terrains, in Daly, J.S., et al., eds., *Evolution of metamorphic belts: Geological Society Special Publication*, v. 43, p. 117–129.
- Kingsbury, J.A., Miller, C.F., Wooden, J.L., and Harrison, T.M., 1993, Monazite paragenesis and U-Pb systematics in rocks of the eastern Mojave Desert, California, U.S.A.: Implications for thermochronometry: *Chemical Geology*, v. 110, p. 147–167, doi: 10.1016/0009-2541(93)90251-D.

- Kohn, M.J., and Malloy, M.A., 2004, Formation of monazite via prograde metamorphic reactions among common silicates: Implications for age determinations: *Geochimica et Cosmochimica Acta*, v. 68, p. 101–113, doi: 10.1016/S0016-7037(03)00258-8.
- Kohn, M.J., and Spear, F., 2000, Retrograde net transfer reaction insurance for pressure-temperature estimates: *Geology*, v. 28, p. 1127–1130, doi: 10.1130/0091-7613(2000)28<1127:RNTRIF>2.0.CO;2.
- Kohn, M.J., Spear, F.S., and Valley, J.W., 1997, Dehydration-melting and fluid recycling during metamorphism: Rangely Formation, New Hampshire, U.S.A.: *Journal of Petrology*, v. 38, p. 1255–1277, doi: 10.1093/ptrology/38.9.1255.
- Kohn, M.J., Catlos, E.J., Ryerson, F.J., and Harrison, T.M., 2001, Pressure-temperature-time path discontinuity in the Main Central thrust zone, central Nepal: *Geology*, v. 29, p. 571–574, doi: 10.1130/0091-7613(2001)029<0571:PTTDPDI>2.0.CO;2.
- Kohn, M.J., Wieland, M.S., Parkinson, C.D., and Upreti, B.N., 2005, Five generations of monazite in Langtang gneisses: Implications for chronology of the Himalayan metamorphic core: *Journal of Metamorphic Geology*, v. 23, p. 399–406, doi: 10.1111/j.1525-1314.2005.00584.x.
- Koons, P.O., 1995, Modeling the topographic evolution of collisional belts: Annual Review of Earth and Planetary Sciences, v. 23, p. 375–408, doi: 10.1146/annurev.ea.23.050195.002111.
- Koons, P.O., Crow, D., Cox, S.C., Upton, P., Templeton, A.S., and Chamberlain, C.P., 1998, Fluid flow during active oblique convergence: A Southern Alps model from mechanical and geochemical observations: *Geology*, v. 26, p. 159–162, doi: 10.1130/0091-7613(1998)026<0159:FFDAOC>2.3.CO;2.
- Koons, P.O., Zeitler, P.K., Chamberlain, C.P., Crow, D., and Meltzer, A.S., 2002, Mechanical links between erosion and metamorphism in Nanga Parbat, Pakistan Himalaya: *American Journal of Science*, v. 302, p. 749–773, doi: 10.2475/ajs.302.9.749.
- Lee, J., Hacker, B.R., Dinklage, W.S., Wang, Y., Gans, P., Calvert, A., Wan, J.L., Chen, W.J., Blythe, A.E., and McClelland, W., 2000, Evolution of the Kangmar Dome, southern Tibet: structural, petrologic and thermochronologic constraints: *Tectonics*, v. 19, p. 872–895, doi: 10.1029/1999TC001147.
- Leloup, P.H., and Kienast, J.-R., 1993, High-temperature metamorphism in a major strike-slip shear zone: The Ailao Shan-Red River, People's Republic of China: *Earth and Planetary Science Letters*, v. 118, p. 213–234, doi: 10.1016/0012-821X(93)90169-A.
- Liu, Y., and Zhong, D., 1997, Petrology of high-pressure granulites from the eastern Himalayan syntaxis: *Journal of Metamorphic Geology*, v. 15, p. 451–466, doi: 10.1111/j.1525-1314.1997.00033.x.
- Ludwig, K.R., 2001, *Squid, A user's manual*: Berkeley, Geochronology Center Special Publication No. 2.
- Ludwig, K.R., 2003, *Isoplot 3.00, A geochronological toolkit for Microsoft Excel*: Berkeley Geochronology Center Special Publication No. 4.
- Malloy, M., 2004, Rapid erosion at the Tsangpo knickpoint and exhumation of southeastern Tibet [M.S. thesis]: Lehigh University, 82 p.
- Maluski, H., Matte, P., and Brunel, M., 1988, $^{40}\text{Ar}/^{39}\text{Ar}$ dating of metamorphic and plutonic events in the North and High Himalaya belts (southern Tibet-China): *Tectonics*, v. 7, p. 299–326, doi: 10.1029/TC007i002p00299.
- Mezger, K., Rawnsley, C.M., Bohlen, S.R., and Hanson, G.N., 1991, U-Pb garnet, titanite, monazite, and rutile ages: Implications for the duration of high-grade metamorphism and cooling histories, Adirondack Mountains, New York: *The Journal of Geology*, v. 99, p. 415–428.
- Overstreet, W.C., 1967, The geologic occurrence of monazite: U.S. Geological Survey Professional Paper 530, 327 p.
- Parrish, R.R., 1990, U-Pb dating of monazite and its application to geological problems: *Canadian Journal of Earth Sciences*, v. 27, p. 1431–1450.
- Poage, M.A., Chamberlain, C.P., and Crow, D., 2000, Massif-wide metamorphism and fluid evolution at Nanga Parbat, northern Pakistan: *American Journal of Science*, v. 300, p. 463–482, doi: 10.2475/ajs.300.6.463.
- Powell, R., and Holland, T.J.B., 1988, An internally consistent dataset with uncertainties and correlations: 3. Applications to geobarometry, worked examples and a computer program: *Journal of Metamorphic Geology*, v. 6, p. 173–204, doi: 10.1111/j.1525-1314.1988.tb00415.x.
- Powell, R., and Holland, T.J.B., 1994, Optimal geothermometry and geobarometry: *American Mineralogist*, v. 79, p. 120–133.
- Pyle, J.M., and Spear, F.S., 1999, Yttrium zoning in garnet: Coupling of major and accessory phases during metamorphic reactions: *Geological Materials Research*, v. 1, p. 1–49.
- Pyle, J.M., and Spear, F.S., 2003, Four generations of accessory-phase growth in low-pressure migmatites from SW New Hampshire: *American Mineralogist*, v. 88, p. 338–351.
- Pyle, J.M., Spear, F.S., Rudnick, R.L., and McDonough, W.F., 2001, Monazite-xenotime-garnet equilibrium in metapelites and a new monazite-garnet thermometer: *Journal of Petrology*, v. 42, p. 2083–2107, doi: 10.1093/ptrology/42.11.2083.
- Ratschbacher, L., Frisch, W., Chen, C.S., and Pan, G.T., 1992, Deformation and motion along the southern margin of the Lhasa Block prior to and during the India-Asia collision: *Journal of Geodynamics*, v. 16, p. 21–54, doi: 10.1016/0264-3707(92)90017-M.
- Ratschbacher, L., Frisch, W., and Liu, G., 1994, Distributed deformation in southern and western Tibet during and after the India-Asia collision: *Journal of Geophysical Research*, v. 99, p. 19,917–19,945, doi: 10.1029/94JB00932.
- Royden, L.H., 1996, Coupling and decoupling of crust and mantle in convergent orogens: implications for strain partitioning in the crust: *Journal of Geophysical Research*, v. 101, p. 17,679–17,705, doi: 10.1029/96JB00951.
- Royden, L.H., Burchfiel, B.C., King, R.W., Wang, E., Chen, Z., Shen, F., and Liu, Y., 1997, Surface deformation and lower crustal flow in eastern Tibet: *Science*, v. 276, p. 788–790, doi: 10.1126/science.276.5313.788.
- Schärer, U., 1984, The effect of initial ^{230}Th disequilibrium in young U-Pb ages, the Makalu case, Himalaya: *Earth and Planetary Science Letters*, v. 67, p. 191–204, doi: 10.1016/0012-821X(84)90114-6.
- Schärer, U., Xu, R.H., and Allegre, C.J., 1984, U-Pb geochronology of Gangdese (Transhimalaya) plutonism in the Lhasa-Xigaze region, Tibet: *Earth and Planetary Science Letters*, v. 69, p. 311–320, doi: 10.1016/0012-821X(84)90190-0.
- Schneider, D.A., Edwards, M.A., Kidd, W.S.F., Khan, M.A., Seeber, L., and Zeitler, P.K., 1999, Tectonics of Nanga Parbat, western Himalaya: Synkinematic plutonism within doubly-vergent shear zones of a crustal-scale pop-up structure: *Geology*, v. 27, p. 999–1002, doi: 10.1130/0091-7613(1999)027<0999:TNPWHS>2.3.CO;2.
- Scott, D.J., and St-Onge, M.R., 1995, Constraints on Pb closure temperature in titanite based on rocks from the Ungava Orogen, Canada: Implications for U-Pb geochronology and P-T-t path determinations: *Geology*, v. 23, p. 1123–1126, doi: 10.1130/0091-7613(1995)023<1123:COPCTI>2.3.CO;2.
- Selverstone, J., and Chamberlain, C.P., 1990, Apparent isobaric cooling paths from granulites: Two counter-examples from British Columbia and New Hampshire: *Geology*, v. 18, p. 307–310, doi: 10.1130/0091-7613(1990)018<0307:AICPFG>2.3.CO;2.
- Shen, F., Royden, L.H., and Burchfiel, B.C., 2001, Large-scale crustal deformation of the Tibetan Plateau: *Journal of Geophysical Research*, v. 106, p. 6793–6816, doi: 10.1029/2000JB900389.
- Singh, S.K., and France-Lanord, C., 2002, Tracing the distribution of erosion in the Brahmaputra watershed from isotopic compositions of stream sediments: *Earth and Planetary Science Letters*, v. 202, p. 645–662, doi: 10.1016/S0012-821X(02)00822-1.
- Smith, H.A., and Barreiro, B., 1990, Monazite U-Pb dating of staurolite grade metamorphism in pelitic schists: *Contributions to Mineralogy and Petrology*, v. 105, p. 602–615, doi: 10.1007/BF00302498.
- Smith, H.A., Chamberlain, C.P., and Zeitler, P.K., 1992, Documentation of Neogene regional metamorphism in the Himalayas of Pakistan using U-Pb in monazite: *Earth and Planetary Science Letters*, v. 113, p. 93–105, doi: 10.1016/0012-821X(92)90213-F.
- Spear, F.S., 1991, On the interpretation of peak metamorphic temperatures in light of garnet diffusion during cooling: *Journal of Metamorphic Geology*, v. 9, p. 379–388, doi: 10.1111/j.1525-1314.1991.tb00533.x.
- Spear, F.S., 1993, *Metamorphic phase equilibria and pressure-temperature-time paths*: Washington, D.C., Mineralogical Society of America, 799 p.
- Spear, F.S., and Florence, F.P., 1992, Thermobarometry in granulites: Pitfalls and new approaches: *Journal of Precambrian Research*, v. 55, p. 209–241, doi: 10.1016/0301-9268(92)90025-J.
- Spear, F.S., and Kohn, M.J., 1996, Trace element zoning in garnet as a monitor of crustal melting: *Geology*, v. 24, p. 1099–1102, doi: 10.1130/0091-7613(1996)024<1099:TEZIGA>2.3.CO;2.
- Spear, F.S., and Peacock, S.M., 1989, *Metamorphic pressure-temperature-time paths*, in American Geophysical Union Short Course Geology, v. 7: Washington, D.C., American Geophysical Union, p. 1–25.
- Spear, F.S., and Pyle, J.M., 2002, Apatite, monazite, and xenotime in metamorphic rocks, in Kohn, M.J., Rakovan, J., and Hughes, J.M., eds., *Phosphates: Geochemical, geobiological and materials importance: Reviews in Mineralogy and Geochemistry*, v. 48, p. 293–335.
- Stacey, J.S., and Kramers, J.D., 1975, Approximation of terrestrial lead isotopic evolution by a two-stage model: *Earth and Planetary Science Letters*, v. 26, p. 207–221, doi: 10.1016/0012-821X(75)90088-6.
- Teufel, S., and Heinrich, W., 1997, Partial resetting of the U-Pb isotope system in monazite through hydrothermal experiments: An SEM and U-Pb isotope study: *Chemical Geology*, v. 137, p. 273–281, doi: 10.1016/S0009-2541(96)00161-1.
- Tilton, G.R., and Grunfelder, M.H., 1968, Titanite: Uranium-lead ages: *Science*, v. 159, p. 1458–1461, doi: 10.1126/science.159.3822.1458.
- Townsend, K.J., Miller, C.F., D'Andrea, J.L., Ayers, J.C., Harrison, T.M., and Coath, C.D., 2001, Low temperature replacement of monazite in the Ireteba granite, southern Nevada: geochronological implications: *Chemical Geology*, v. 172, p. 95–112, doi: 10.1016/S0009-2541(00)00238-2.
- Treloar, P.J., Pottis, G.J., Wheeler, J., and Rex, D.C., 1991, Structural evolution and asymmetric uplift of the Nanga Parbat Syntaxis, Pakistan Himalaya: *International Journal of Earth Sciences*, v. 80, p. 411–428.
- Tuccillo, M.E., Essene, E.J., and Van der Pluijm, B.A., 1990, Growth and retrograde zoning in garnets from high-grade metapelites: Implications for pressure-temperature paths: *Geology*, v. 18, p. 839–842, doi: 10.1130/0091-7613(1990)018<0839:GARZIG>2.3.CO;2.
- Tucker, R.D., Raheim, A., Krogh, T.E., and Corfu, F., 1987, Uranium-lead zircon and titanite ages from the northern portion of the Western Gneiss Region, south-central Norway: *Earth and Planetary Science Letters*, v. 81, p. 203–211, doi: 10.1016/0012-821X(87)90156-7.
- Vannay, J.-C., Grasemann, B., Rahn, M., Frank, W., Carter, A., Baudraz, V., and Cosca, M., 2004, Miocene to Holocene exhumation of metamorphic crustal wedges in the NW Himalaya: Evidence for tectonic extrusion coupled to fluvial erosion: *Tectonics*, v. 23, p. TC1014, doi: 10.1029/2002TC001429.
- Wang, E., and Burchfiel, B.C., 1997, Interpretation of Cenozoic tectonics in the right-lateral accommodation zone between the Ailao Shan shear zone and the eastern Himalayan syntaxis: *International Geology Review*, v. 39, p. 191–219.
- Whittington, A.G., Harris, N.B.W., and Butler, R.W.H., 1999, Contrasting anatectic styles at Nanga Parbat, northern Pakistan, in Macfarlane, A., Sorkhabi, R.B., and Quade, J., eds., *Himalaya and Tibet: Mountain roots to mountain tops*: Boulder, Colorado, Geological Society of America Special Paper, v. 328, p. 129–144.
- Williams, I.S., 1998, U-Th-Pb geochronology by ion microprobe, in McKibben, M.A., Shanks, W.C., III, and Ridley, W.E., eds., *Applications of microanalytical techniques to understanding mineralizing processes: Reviews in Economic Geology*, v. 7, p. 1–35.
- Wing, B.A., Ferry, J.M., and Harrison, T.M., 2003, Prograde destruction and formation of monazite and allanite

- during contact and regional metamorphism of pelites: *Petrology and Geochronology: Contributions to Mineralogy and Petrology*, v. 145, p. 228–250.
- Yin, A., Harrison, T.M., Ryerson, F.J., Chen, W.J., Kidd, W.S.F., and Copeland, P., 1994, Tertiary structural evolution of the Gangdese Thrust System, southeastern Tibet: *Journal of Geophysical Research*, v. 99, p. 18,175–18,201, doi: 10.1029/94JB00504.
- Yin, A., Harrison, T.M., Murphy, M.A., Grove, M., Nie, S., Ryerson, F.J., Xiaofeng, W., and Zengle, C., 1999, Tertiary deformation history of southeastern and southwestern Tibet during the Indo-Asian collision: *Geological Society of America Bulletin*, v. 111, p. 1644–1664, doi: 10.1130/0016-7606(1999)111<1644:TDHOSA>2.3.CO;2.
- Yin, A., Dubey, C.S., Kelty, T.K., Gehrels, G.E., Chou, C.Y., Grove, M., and Lovera, O., 2006, Structural evolution of the Arunachal Himalaya and implications for asymmetric development of the Himalayan orogen: *Current Science*, v. 90, p. 195–206.
- Zeitler, P.K., 1985, Cooling history of the NW Himalaya, Pakistan: *Tectonics*, v. 4, p. 127–151, doi: 10.1029/TC004i001p00127.
- Zeitler, P.K., Sutter, J.F., Williams, I.S., Zartman, R.E., and Tahirkheli, R.A.K., 1989, Geochronology and temperature history of the Nanga Parbat-Haramosh Massif, Pakistan, in Malinconico, L.L., Jr., and Lillie, R.J., eds., *Tectonics of the western Himalayas*: Boulder, Colorado, Geological Society of America Special Paper, v. 232, p. 1–22.
- Zeitler, P.K., and Chamberlain, C.P., 1991, Petrogenic and tectonic significance of young leucogranites from the north-west Himalaya, Pakistan: *Tectonics*, v. 10, p. 729–741.
- Zeitler, P.K., Chamberlain, C.P., and Smith, H., 1993, Synchronous anatexis, metamorphism, and rapid denudation at Nanga Parbat, Pakistan Himalaya: *Geology*, v. 21, p. 347–350, doi: 10.1130/0091-7613(1993)021<0347:SAMARD>2.3.CO;2.
- Zeitler, P.K., Meltzer, A.S., Koons, P.O., Craw, D., Hallet, B., Chamberlain, C.P., Kidd, W.S.F., Park, S.K., Seeber, L., Bishop, M., and Shroder, J., 2001a, Erosion, Himalayan geodynamics, and the geomorphology of metamorphism: *GSA Today*, v. 11, no. 1, p. 4–8, doi: 10.1130/1052-5173(2001)011<0004:EHGATG>2.0.CO;2.
- Zeitler, P.K., Koons, P.O., Bishop, M.P., Chamberlain, C.P., Craw, D., Edwards, M.A., Hamidullah, S., Jan, M.Q., Khan, M., Khattak, M., Kidd, W.S.F., Mackie, R.L., Meltzer, A.S., Park, S.K., Pecher, A., Poage, M.A., Sarker, G., Schneider, D.A., Seeber, L., and Shroder, J.F., 2001b, Crustal reworking at Nanga Parbat, Pakistan; metamorphic consequences of thermal-mechanical coupling facilitated by erosion: *Tectonics*, v. 20, p. 712–728, doi: 10.1029/2000TC001243.
- Zeitler, P.K., Malloy, M.A., Kutney, M.P., Idleman, B.D., Liu, Y., Kidd, W.S.F., and Booth, A.L., 2006, Geochronologic evidence for the tectonic and topographic evolution of SE Tibet: *Eos (Transactions, American Geophysical Union)*, v. 87, Abstract T23B-0480.
- Zhang, L.-S., and Schärer, U., 1996, Inherited Pb components in magmatic titanite and their consequence for the interpretation of U-Pb ages: *Earth and Planetary Science Letters*, v. 138, p. 57–65, doi: 10.1016/0012-821X(95)00237-7.
- Zhang, L.-S., and Schärer, U., 1999, Age and origin of magmatism along the Cenozoic Red River shear belt, China: *Contributions to Mineralogy and Petrology*, v. 134, p. 67–85, doi: 10.1007/s004100050469.
- Zhang, Y.-Q., Dai, T.-M., and Hong, A.-S., 1981, Isotopic geochronology of granitoid rocks in southern Xizang plateau, in *Symposium Proceedings, Qinghai Xizang (Tibet) plateau*: Beijing, Chinese Science Press, p. 483–495.
- Zhang, Z.G., Liu, Y.H., Qnag, H.X., and Xu, B.C., 1992, *Geology of the Namche Barwa region*: Beijing, Chinese Science Press, 185 p.
- Zhong, D., and Ding, L., 1996, Discovery of high-pressure basic granulites in Namjagbarwa area, Tibet, China: *Chinese Science Bulletin*, v. 41, p. 87–88.
- Zhu, X.K., O’Nions, R.K., Belshaw, N.S., and Gibb, A.J., 1997, Significance of in situ SIMS chronometry of zoned monazite from the Lewisian granulites, NW Scotland: *Chemical Geology*, v. 135, p. 35–53, doi: 10.1016/S0009-2541(96)00103-9.

MANUSCRIPT RECEIVED 17 MAY 2006
 REVISED MANUSCRIPT RECEIVED 21 MARCH 2008
 MANUSCRIPT ACCEPTED 29 MARCH 2008

Printed in the USA